Study of Extreme Events in Millennial Aerosol Records from Greenland

Master thesis
Faculty of Science, University of Bern

handed in by

Kathrine Mia Link

2020

Supervisor

Prof. Dr. H. Fischer

Dr. T. Erhardt

The amount of work for this master thesis is 30 ECTS.
Another 30 ECTS were acquired in an internship.

Abstract

Greenland ice-core aerosol records give us a unique opportunity to study changes in past climatic conditions. These records are important for climate reconstruction and past changes in source regions. Impurities in the ice from aerosols can reveal information about wildfires, volcanic eruptions, storminess, and aerosol transport. We measured the annual scale aerosol variability of different aerosol types from a shallow ice core (EGRIP S6) from Northeast Greenland for the period of the last 1 000 years with a high-resolution Continuous Flow Analysis System. The aerosol record was then dated by using volcanic marker horizons in the ice. Annual layers could be identified by using the Straticounter algorithm. Further, we conducted trend analysis which revealed a trend in conductivity from 1840 to 2001 AD and in nitrate from 1933 to 2001 AD which we related to anthropogenic emissions. We examined extreme events and their frequency of occurrence in the ice core record by using extreme value analysis. We validated our threshold approach by comparing the extreme events found in the conductivity to historical volcano eruptions. Distinct peaks in ammonium are attributable to large wildfire events. Overall, the small number of extreme event occurrence made it impossible to link their occurrence to atmospheric circulation. Further, we correlated the EGRIP S6 sodium aerosol record with the sodium aerosol record of Tunu and NEGIS. Our results showed that on an interannual timescale regional weather and post depositional effect have a strong influence on inter site variability. This is in line with other studies. Furthermore, we tried to identify changes in interannual to multidecadal climate indices influencing the atmospheric dynamics depicted in the ice core record. We did this by directly correlating the AMO, NAO and PDO index to the ice core record. As a result, we only found weak correlations with the aerosol record expect for the long AMO index which covers the entire time period of the ice core record. A significant correlation in calcium and sodium could be attributed to the multidecadal trend shown in the AMO which is depicted in the ice core record. For the correlation of NAO and the ice core record, our results showed that on an interannual timescale regional weather and post depositional effect have a strong influence. We suggest replicate coring in a defined distance to increase the representativeness of the combined records to be able to detect atmospheric circulation in the ice core record and draw conclusions about changes in transportation pathway to the Northeast Greenland region.

Table of Contents

1 Introduction

Greenland ice core aerosol records give us a unique opportunity to study changes in past climatic conditions. They are crucial for understanding the present climate change, but also reveal sub seasonal information of the past climate. The impurities in the ice, originating from aerosols, reveal information on wildfires, volcanic eruptions, storminess as well as on the aerosol transport of the individual aerosols. Extreme events have received increasing attention, but have barely been studied in the ice core record so far. Therefore, in this work statistical analysis of extreme events is conducted on different impurities of the EGRIP S6 ice core from Northeast Greenland. The frequency of extreme events is determined and potential influences of changes in Calcium (Ca), Sodium (Na), Ammonium (NH_4^+) and Nitrate (NO_3^-) on changes in atmospheric circulation patterns are investigated. Additionally, we compare the EGRIP S6 sodium record with the Tunu and NEGIS ice core sodium record.

1.1 The Ice Core Aerosol Record

Ice core aerosol records include insoluble mineral dust, sea salt, and biogenic aerosols. These markers can either be directly emitted from a source (primary formation) or from gaseous precursors by secondary aerosol formation in the atmosphere (Pandis & Seinfeld, 2006). Their concentrations vary because of multifactorial changes. These changes can be in aerosol emission at the source, in the atmospheric transport velocity and pathway and in aerosol deposition en route and over the ice sheet. In other words, there is no direct relation between the atmospheric concentration and the contaminant concentration in the ice. Particles can be deposited via wet or dry deposition. With constant atmospheric concentrations, an increase in snow accumulation also increases the flux of contaminants to the ice sheet. However, in the accumulated snow, the concentration of that contaminant decreases because of dilution of dry deposited aerosol in the snow (Alley et al., 1995). Additionally, snow drifting by surface wind and sublimation can change the composition at the deposition site. In order to get a better understanding of these processes we measured impurity contents like Ca, Na, NH_4^+, NO_3^- and dust particles, including their size. Additionally, we detected other properties, namely, electrolytic conductivity (σ), acidity and $\delta^{18}O$ of the ice.

As impurity concentrations in the ice are generally very low, contamination during handling and analysis poses a high risk for measurement errors. In order to avoid this, we use the high-resolution Continuous Flow Analysis (CFA) system of the University of Bern. This is a highly sensitive and contamination free sampling and measurement system to generate continuous, high-resolution data (Bigler et al., 2011; Kaufmann et al., 2008; Röthlisberger et al., 2000). A description of the Bernese CFA System will be given in Chapter 2. The StratiCounter approach, an automated algorithm, by Winstrup et al. (2012) uses the seasonal variation in the aerosols to identify annual layers. Historically known eruptive volcanoes are used to date the ice core record. An explanation of the age scale is given in Chapter 2. In Chapter 3, extreme events are identified. Furthermore, the ice core record is related to

multidecadal oceanic and interannual atmospheric circulation patterns as well as other ice core records by statistical analysis. In Chapter 4, a discussion on the findings is provided and put into perspective with other ice core studies, which have been made so far.

1.2 Aerosol Transport to Greenland

The major feature of large-scale atmospheric circulation around Greenland is the westerly jet stream. Aerosols are transported via large-scale atmospheric circulation patterns from their source region to the deposition site in Greenland. This long-distance transport around the globe takes place via the jet stream. The pathway of storm tracks over Greenland is determined by the position of the jet stream. Hutterli et al. (2005) and Merz et al., (2013) state that accumulation variability in northeastern Greenland is mostly influenced by cyclones origination from the Greenland Sea. The prevailing cyclonic flow system associated with air transport to Greenland originates from the south of Greenland and is associated with a blocking situation over northeastern Europe. Therefore, the dominant factor of the variations in the aerosol concentration ice core records in northeastern Greenland region originates from changes in cyclonic activity. Cyclonic activity over Greenland increases with northerly storm tracks when the position of the jet stream is moving northwards. This is mainly caused by two reasons and leads to low precipitation in the northeastern part of Greenland. Firstly, this region is located on the leeward site of the ice divide making it more difficult to be reached by westward flowing moist air masses. Secondly, orographic uplift as well as the prevailing anticyclonic system over the center of the Greenland ice sheet prohibits moist air masses from entering the interior region (Hobbs, 1945; Roe, 2005). The aerosols are then deposited via dry or wet deposition in stratified layers onto the Greenland ice sheet. Before all this can take place, the aerosols need to be uplifted from their source region and included in the atmospheric circulation. Different aerosols have different sources and therefore originate from different regions. By following the transport path back with air mass trajectories several source regions are determined by Kahl et al. (1997). In the following, the investigated tracers are introduced and the sources described.

The conductivity σ is a measure of the total amount of ions dissolved in a liquid. Here it represents the total amount of dissolved aerosol ions in the melt water as a baseline with superimposed distinct spikes coming from sulfuric acid depositions mainly from volcanic eruptions and ammonium depositions from large wildfire events.

Sea salt is the main source of Na in the Greenland ice core records (Legrand & Mayewski, 1997). It mainly originates from the North Atlantic Ocean through bubble bursting at the wave surface or from sea ice over the North Atlantic (Wagenbach et al., 1998; Yang et al. , 2008). Storms in the North Atlantic region transport it to Greenland. Therefore, variations in Na concentration can be caused by a change of wind speed directly above the ocean, by changes in sea ice cover, and by brine and frost flower formation on the ice sheet (Fischer et al., 2007; Legrand & Mayewski, 1997). The Na peaks are found in winter since storminess over the North Atlantic is

highest in this season. Rhodes et al. (2018) found that for central Greenland sites on interannual timescales the influence of meteorology on aerosol transport and the deposition is dominant for interannual variability in the Na record. Therefore, ice cores from this region may record the influence of meteorological changes on interannual timescales.

Calcium aerosol is mainly produced by chemical and physical weathering of crustal material. Therefore, it can be seen as a mineral dust tracer. Dust has a major influence on oceanic biogeochemistry as well as on the radiative balance. The air mass trajectories of mineral dust originate in the Asian deserts providing the main source of the concentrations of Ca in the ice cores (Bory et al. , 2002; Svensson et al., 2006). Biscaye et al. (1997) and Bory et al. (2003) identified the Taklamakan desert in China being the most active dust source at the moment. This is confirmed by chemical analysis of the mineral dust (Biscaye et al., 1997; Bory et al., 2002, 2003). The Taklamakan desert is surrounded by high mountains. The successive cold fronts pass East Asia caused by instability of synoptic systems over the Pacific Ocean and East Asia (Sun et al., 2001). These storms coincide with the Ca spring peak and are associated with these north-westerly and northerly winter-monsoon winds (Bory et al., 2003). Those frontal systems produce storms entering the Taklamakan desert from a corridor in the east blowing dust over the high mountains surrounding the desert region. Through this process, dust particles are able to enter the upper troposphere, where the dust particles are largely protected from scavenging by precipitation. The surface wind speed needs to exceed a certain threshold velocity to be able to uplift the dust. This threshold is a function of soil moisture, grain size, and surface roughness.

The sources of ammonium are nitrogen turnover in soil and the ocean, fertilizer use, animal waste, vegetation as well as wildfires, but there are also marine biogenic sources. The main part is produced by chemical processes in the atmosphere originating from the ammonification of ammonia. Large peaks coming from large boreal wildfires originating mostly from Canadian regions are detected on top of these background NH_4^+ concentrations. These are attributed to large biomass burning events (Fischer et al., 2015; Fuhrer et al., 1996; Legrand et al., 2016). Fuhrer et al. (1996) state that North America is the main source region of ammonium. Ammonium peaks, which occur during May in modern times and July-August in pre-industrial times, are caused by enhanced bacterial decomposition of nitrogen in soils This shift is attributed to anthropogenic aerosol emissions (Gfeller et al., 2014).

Nitrate is produced by oxidation processes of NO_2 and NO, which is released by the soil, by biomass burning, by fossil fuel combustion, and by lightning (Pandis & Seinfeld, 2006). Nitrate peaks in May in modern times and June-July in pre-industrial times. Both, nitrate concentration increase and its shift in seasonality is caused by aerosol increase due to anthropogenic emissions and Artic haze (Gfeller et al., 2014). Nitrate is affected by post-depositional loss since it is reversibly incorporated in the snow surface (Fischer et al., 1998).

1.3 Interannual to multidecadal modes in ocean and atmosphere dynamics

The occurrence of atmospheric patterns is influenced by anomalies in climate parameters such as surface temperatures or sea level pressure. These atmospheric patterns may trigger extreme events and modulate climate variability on spatial as well as temporal scales. The aerosol transport onto Greenland's ice sheet is directly related to storm activity and atmospheric circulation patterns. Therefore, investigating the changes in aerosol concentration in ice cores can lead to a better understanding of the strength of the transport mechanisms (atmospheric circulation) (Fischer, 2001).

The quasi-permanent Icelandic low determines the interannual variability in atmospheric circulation over the North Atlantic. The pressure differences between Iceland and the Azores are reflected in the North Atlantic Oscillation (NAO) index (Hurell, 2001). The NAO has a multiannual variability with a positive index pointing towards stronger westerlies and vice versa. Weaker westerlies over the Atlantic lead to storm tracks moving southward (Hurrell, 1995).Therefore, the NAO can have an influence on the variability of aerosol that are deposited on Greenland. Since sea salt originates from this area, its concentration is strongly affected by the shifts of major storm tracks over the Northern Atlantic and its meridional transport. Fischer (2001) found a weakly significant correlation pattern of sodium concentrations and reanalysis data of sea level pressure (SLP) and 500 mbar pressure in the North Atlantic region. The Na anomalies were related to variations in storm tracks and storm activity over the North Atlantic (Fischer & Mieding, 2005). This is in line with Hutterli et al. (2005) stating that the NAO index has an imprint on the ice accumulation rate. Higher Na concentrations come along with a positive NAO pattern since we find more frequent winter storms with northerly storm tracks (Fischer, 2001; Fischer & Mieding, 2005). Therefore, extratropical teleconnection patterns like the NAO are influencing the variability of Na concentrations. However, the correlation is weak and other variability prohibits to use Na concentrations as a NAO proxy with sufficient skill.

The Pacific Decadal Oscillation (PDO) is a measure for sea surface temperature (SST) anomalies over the northern Pacific Ocean. It is a long-lived interdecadal climate pattern which is associated with El Niño (Grigholm et al., 2009). The PDO has a positive value when SLP is below average over the North Pacific and when SST are anomalously warm along the Pacific Coast and cool in the interior North Pacific. The PDO has a negative value when there are cool SST anomalies along the North American coast and warm SST anomalies in the interior or above average SLP over the North Pacific (Mantua & Hare, 2002). Anomalies in the PDO, the El Niño and the Arctic Oscillation (AO) patterns cause droughts that lead to a higher occurrence of extensive wildfires in the North American continent (Leuenberger, 2013). This could lead to high NH_4^+ concentration in the ice core record.

Fischer and Mieding (2005) performed Monte Carlo singular spectrum analysis to be able to detect decadal to multidecadal variability related to sea salt concentration. Sea salt production is not causally connected to SST, however, it is indirectly affected by pressure distribution and storm activity over the North Atlantic. The Atlantic

Multidecadal Oscillation (AMO) is a measure of the SST anomalies in the North Atlantic region. It is a teleconnection pattern on multidecadal timescales influencing the atmospheric circulation in the North Atlantic. Therefore, we examine the correlation between the AMO and the ice core record. Long-term variability in atmospheric circulation comes from atmosphere/ocean interaction. There are several explanations on how ocean and atmosphere interact. This interaction has mostly been attributed to variations in the thermohaline circulation induced by long-term variability in SST and sets the stage for changes in multidecadal atmospheric circulation (Delworth & Mann, 2000; Fischer & Mieding, 2005). Fischer and Mieding (2005) found significant variability in North Atlantic SST and SLP on decadal to multidecadal time scales. Therefore, they related a negative anomaly in SST over the North Atlantic to intervals with high sea salt concentration in the northern Greenland region. This comes in line with a SLP anomaly pattern with higher pressure in the eastern Atlantic region and low pressure over the Greenland sea. They claim this deep pressure trough to be connected to enhanced cyclonic activity entering the Greenland ice. The center of action of the NAO, AMO and PDO are shown in Figure 1.

1.4 Inter-annual representativeness of Ice Core Records

Gfeller et al. (2014) studied different ice cores located in the vicinity of the NEEM site. Their work showed that the seasonal coherence of aerosol records between the cores is very high, however, inter-annually it is substantially lower. In addition, the spatial representation decreases with distance to the depositional site. This is attributed to depositional noise caused by unevenly distributed deposition and topographic effects like sastrugi formation during wind reworking. They conclude that replicate coring is the measure to better constrain atmospheric processes and their variability. This effect is especially pronounced in the low accumulation area of Northeast Greenland where the ratio of atmospheric signal to depositional noise is especially low. Therefore, it might not be possible to derive changes in large-scale circulation pattern by using one core only. They argue that 70 % of the inter-annual atmospheric variability can be depicted by using 5 replicate ice cores (Gfeller et al., 2014). Crüger et al. (2004) argue that in local accumulation in Greenland only regional scale features and no large-scale information is represented.

1.5 Data

After the North Greenland Eemian Ice Drilling (NEEM) project, East Greenland Ice Core Project (EGRIP) is the second project in Greenland with the aim of receiving an ice core with a reliable Holocene and late-glacial climate record (Fig. 2). Furthermore, since EGRIP is located on a fast flowing ice stream, the objective is to better understand and to predict glacier flow dynamics. During the field campaign shallow ice cores like the S6 were drilled in addition to the deep ice core project. The EGRIP S6 ice core was drilled to construct in situ physical property measurements. After the field work, we used the Bern CFA System to continuously measure impurities in the ice.

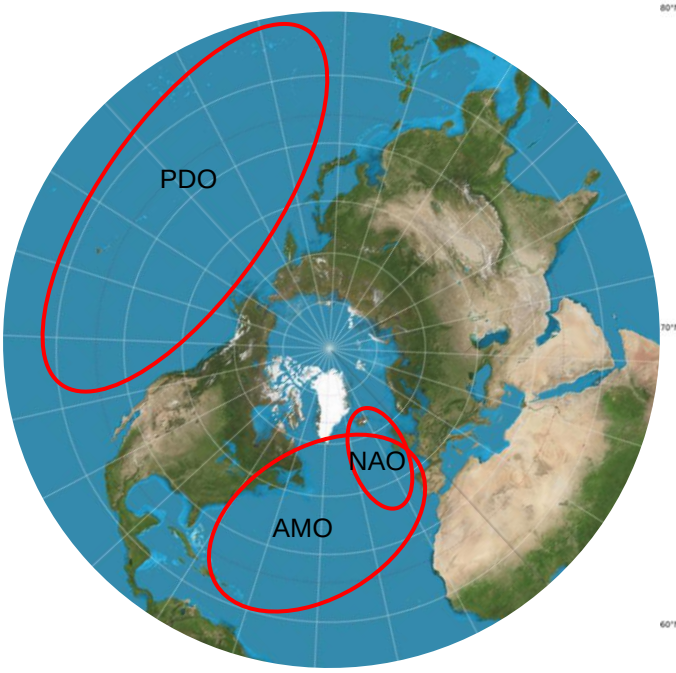

Figure 2 Potential center of actions of the NAO, AMO and the PDO index. Source: https://en.wikipedia.org/wiki//File:Stereographic_projection_SW.JPG.

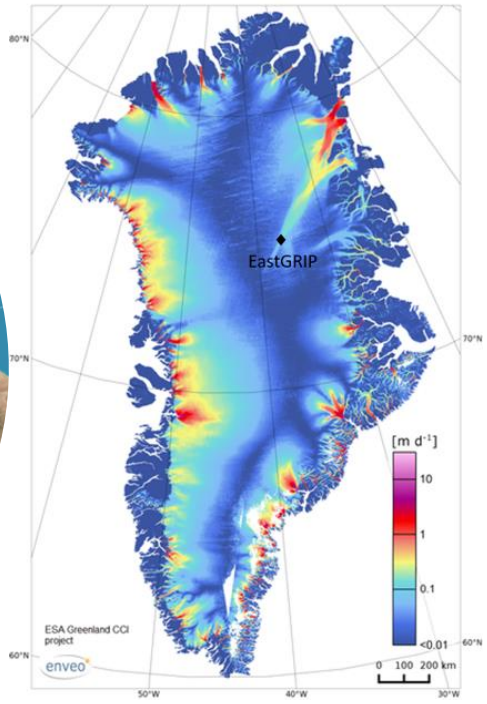

Figure 1 Location of the Greenland ice core drilling site EGRIP depicting the flow rate of the Greenland ice sheet from interferometric synthetic aperture radar data. The ice divide is indicated by the lowest flow rate in the center of Greenland approximately going from the North to the South of Greenland. Source: http://www.enveo.at/products.

The EGRIP study site is located at (75°62′N, 35°97′W, 2702 m asl) in central, northeastern Greenland on the eastern side of the ice divide (Fig. 2) (Du et al., 2019). During the field campaign in 2018 a shallow 140 m long ice core (EGRIP S6) was drilled in northeast Greenland in the vicinity of the study site. The accumulation rate is estimated to be 0.11 m per year ice equivalent based on annual layer counting on the Northeast Greenland Ice Stream shallow ice core (Vallelonga et al., 2014). We measured the S6 core from a snow pit depth of about 2 m beneath the surface to the bottom at about 140 m depth.

1.6 Goal and Objectives

The goal of this Master thesis is to retrieve and interpret the annual to multiannual scale aerosol variability for different aerosol species from a shallow ice core taken from northeast Greenland. The focus of this work is on the high-resolution aerosol record of this dataset, which roughly covers the last 1000 years in time. The overall study is thus divided into an experimental part and a data interpretation part.

After the ice core was cut in a cold lab, we measured the aerosol concentrations, and dated the resulting record using cross dating techniques. This was done with other ice cores by using volcanic horizons in the ice and an annual layer counting algorithm. The statistical analysis of extreme events in the ice core record was conducted to look at their frequency and link potential influences of changes in σ, Ca, Na, NH_4^+ and NO_3^- to changes in atmospheric circulation patterns. As a final step,

the EGRIP S6 ice core sodium record was compared to the Tunu and NEGIS sodium record.

2 Methods

The data acquisition and evaluation followed a step-wise approach. First, we measured the ice core record by using the University of Bern CFA system to generate a continuous, high resolution data set. Afterwards, we used volcanic marker horizons and the StratiCounter approach by Winstrup et al. (2012) to get to an absolute age scale and annual layer boundaries. We then applied extreme value analysis to the data. As a final step, we compared the sodium record to other ice cores sodium records and correlated atmospheric and oceanic circulation patterns with different impurities. In the following these steps are described in more detail.

2.1 The University of Bern CFA system

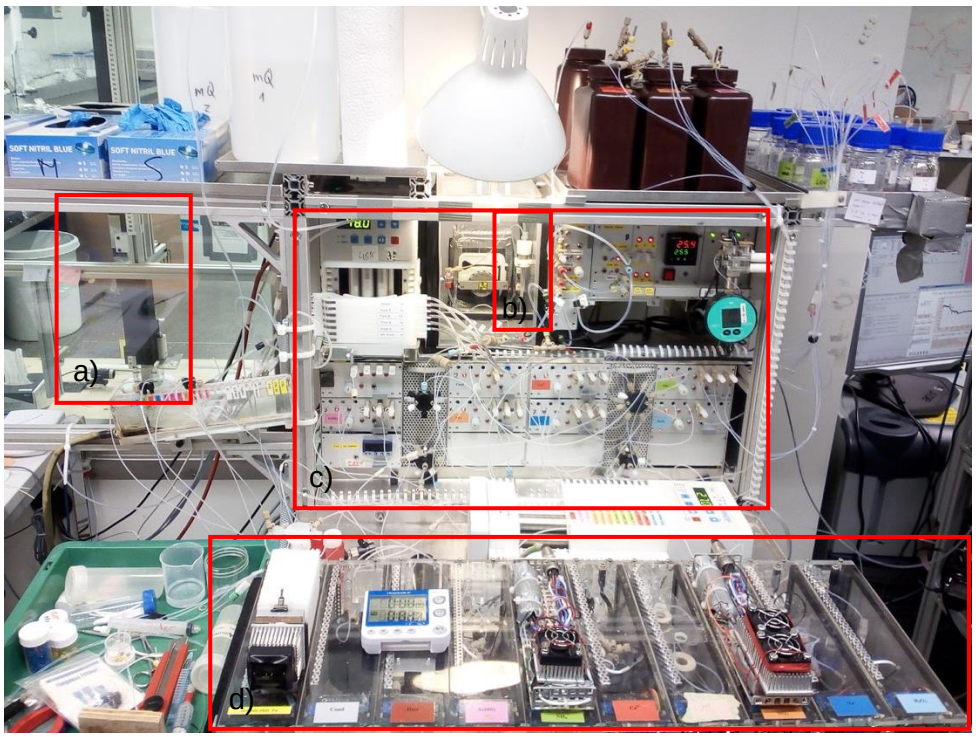

Figure 3 The CFA system with (a) melt unit, (b) debubbler integrated in (c) the distribution unit and (d) the analysis unit.

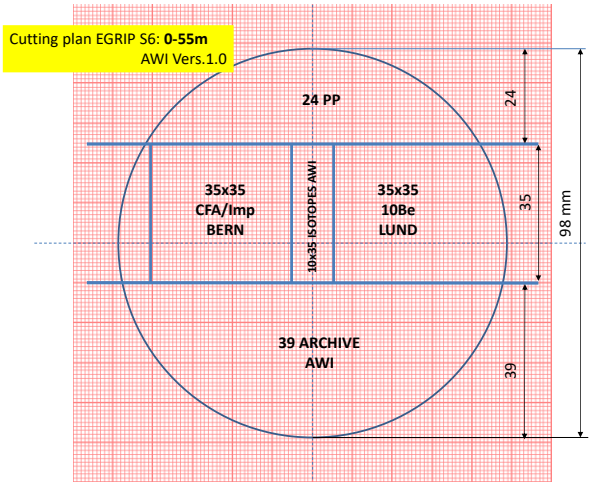

Figure 4 Cutting Plan EGRIP S6 with the CFA Bern piece on the left side.

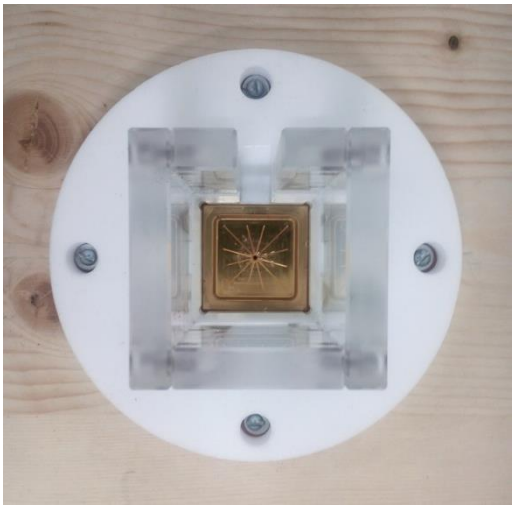

Figure 5 The melter head.

The University of Bern CFA system consists of a melting, sample distribution, and analysis unit (Fig. 3). In order to retrieve the aerosol concentration, we first cut the ice core sample in a cold lab to receive a longitudinal subsection with a squared cross section of 35x35 mm and a length of 100 mm. The cutting plan is given in Figure 4. Since no drilling fluid was used to obtain the S6 ice core, major breaks especially in the lower meters of the ice core could not be avoided. With depth the hydrostatic pressure in the ice increases, leading to a closure of the borehole. 6m of the ice core could not be measured, because the box containing this part was dropped during its transport. This resulted in fragmented ice and led to ice pieces that were too short to be measured in the CFA system. After cutting, we cleaned surface breaks with clean blades to avoid contamination that are mainly caused by the handling of the ice with gloves. Then, the ice was melted and the innermost part of the ice core was pumped to the distribution unit and measured in the analysis unit. Therefore, we were able to analyze contamination free, pristine ice.

2.1.1 Melting Unit

The melting unit was located in a cold lab with temperatures below -20°C to prevent the ice from unintentional melting. We continuously melted the ice on a square, gold plated melter head (Fig. 5) to receive sample water to measure the impurity content. Therefore**,** the ice slab was placed vertically into the mounting system. Gravitation drew the ice slab downwards in the direction of the melter head, where it was melted with a melt speed of approximately 3 cm min^{-1}. However, the analysis system is only able to function under the condition of receiving a minimum flux of melt water. The amount of melt water is not sufficiently high for the uppermost part of the ice core, which consists of firn that has a lower density than ice. The melt rate is therefore faster in this region. The following CFA system units are further described in Kaufmann et al., (2008).

2.1.2 Distribution Unit

A peristaltic pump moved the fluid to the distribution unit, which is located outside the cold lab in a lab at room temperature. Here, the fluid was distributed to different analysis units and chemically analyzed. Before the liquid enters the analysis unit, a debubbler removes bubbles (Fig. 3) which would disturb the signal system.

2.1.3 Analysis Unit

We measured the concentration of several dissolved chemical constituents, such as Ca^{2+}, NH_4^+, NO_3^-, H_2O_2, and elemental concentrations and size distribution of insoluble particles, as well as the electrolytic conductivity, and pH, with different detectors.

The detection methods for soluble aerosol species were photometric methods, whereas insoluble particles were measured by laser light attenuation and a novel extinction and scattering device. The absorbance detection device measures NO_3^- and pH, the photomultiplier detector measures Ca^{2+}, NH_4^+, H_2O_2 using fluorescence and the conductivity meter measured the electronic conductivity. The so-called Abakus Laser Particle Sizer measured particle concentration and size distribution using light attenuation (Erhardt, 2013). Cavity-ring-down-spectroscopy was used to measure $\delta^{18}O$ and δD. Elemental analyses are enabled by using inductively coupled plasma - mass spectrometry, where the Bern system is using a Time-Of-Flight mass spectrometer to also detect the elemental composition in single dust (Erhardt et al., 2019). For our analysis, we used the Ca and Na record of the Time-Of-Flight mass spectrometer. For further information about the detection methods, please see (Kaufmann et al., 2008), Röthlisberger et al. (2000) and Erhardt et al. (2019).

2.2 Data Acquisition

CFA can be used to measure impurities in high spatial resolution (effective resolution about 1-2 cm). The reason for this range in resolution span is the dispersion in the CFA system, the response time of the detection methods, and the melt speed. In the case of the S6 ice core, this was still in the range of annual layers, which leads to an approximate layer thickness of 0.11 m per year ice equivalent (Vallelonga et al., 2014). This means that annual cycles were detected (Bigler et al., 2011; Kaufmann et al., 2008; Röthlisberger et al., 2000; Sigg et al. 1994).

We calibrated the system before each run and after the last run with standard solutions. This process made it possible to convert voltage signals obtained from the analysis methods to concentrations (Röthlisberger et al., 2000). It is assumed that the mass flow and conductivity sensor retrieve a correct output over their lifespan and were calibrated by the manufacturer. The Abakus Laser Particle Sizer dust sensor was calibrated by Erhardt (2013) with standards of the total size range of interest. For further details on the calibration of the dust sensor, please see Erhardt (2013).

2.3 Data Processing

After the measurement process, it was necessary to process the raw data and check their quality. In order to minimize drift in the data, we calibrated the system in regular intervals. The voltage signal was then converted to concentration with the calibrated data.

The melt water reaches the sensors in the analysis unit at different times due to different setups of the modules. Therefore, we aligned the multicomponent standard peak of all components to determine the delay between injection and detection at the analysis unit. A program written in Labview (National Instruments) processes the raw data and converts it into concentrations in parts per billion water equivalent (Kaufmann et al., 2008). Even though the ice was melted and measured continuously, the voltage signals are received in a discrete time with a frequency of 1 Hz. The time index can be converted to a depth scale knowing the melt rate and the length of the ice slab. To convert the voltage signal to concentration, calibrations with standard solutions of a known concentration are used.

Additionally, we checked for data quality issues because of for example unwanted spikes caused by air bubbles, electronic noise or errors occurring from potentially contaminated break surfaces. These breaks were noted during the sample preparation. We therefore removed a defined interval from the CFA data and a preset interval from the ICP-MS data before and after a break. After the data transformation, we plotted the different components chronologically. To get to a chronological age scale, we merged all measurement runs into one file and transferred it to a continuous depth scale with a resolution of 1 mm.

2.4 Age Scale

Precise and accurate timescales are a necessary prerequisite for any paleoclimatic interpretation and for the comparison with other records. Periodicity and rapidity of the past climate changes can then be studied and compared to those of other locations to be able to retrieve a spatial pattern and relative timing of specific events. With this knowledge, it is also possible to draw conclusions about causes and mechanisms of past climatic changes.

In this study, the different impurity data-series are used after the calibration to generate an age scale for the ice core in a two-step approach. In the first step, signals of well known volcanic eruptions are identified to obtain a rough absolute date (Rasmussen et al., 2013). We took the conductivity dataset to identify major, historically dated volcanic eruptions, which are referred to as match points in the following sections. Due to the concurrent deposition of volcanogenic sulfate, high conductivity values are an indicator for volcanic eruptions. We manually identified those major volcanic eruptions in the EGRIP S6 core and compared them to the EGRIP main core. The drilling location of EGRIP is only about 1.5 km away from EGRIP S6. Therefore, we assume the volcanic peaks to occur in both locations and the EGRIP main core timescale to be a good representative for EGRIP S6.

In a second step, we used a semi-automated approach (StratiCounter, Winstrup et al., 2012) to identify the annual layers for the different aerosol species. Annual layers are defined by an annual seasonal cycle with the maximum concentration representing the layer boundary in the beginning and end of one year. Since the accumulation rate differs from year to year, it is more meaningful to calculate annual means. To be able to calculate those annual means annual layer needed to be retrieved. In order to receive annual layer boundaries, we use the StratiCounter algorithm based on the statistical basis of hidden Markov models to detect annual layers. The StratiCounter algorithm is much faster in processing the data and gives objective uncertainty estimates for the resulting timescales than those produced manually. Therefore, the false discovery and miss rates of a segment being a layer are much lower, and the accumulated age uncertainty is smaller (Winstrup et al., 2012). First, we prepared the data by transferring the measured depth to an ice equivalent depth in order to correct for the density shift from snow to ice. To this end, the data was manually fitted to a firn densification model, the Herron-Langway Model (Herron & Langway, 1980). We assumed an accumulation rate of 12 cm a^{-1} and an annual temperature of 241.15 K. We left out the 6 m gap from 86 to 92 m since it consisted of broken ice and therefore could not be measured. We used chemistry series that show annual cycles and a manually counted initial set of layer boundaries as input data to train the algorithm to understand the typical layer thickness. For the manually counted initial set of layer boundaries, we took the interval reaching from Krakatoa (1883) to Tambora (1816) based on the layers depicted in the Ca record. Ca shows a clear annual cycle with its peak in spring. As output, we receive a probabilistic age estimate along the core and the most likely position of the layer boundaries.

Later, we transferred the data from ice equivalent back to measured depth scale since the match points of both, the EGRIP main core and the EGRIP S6 core, were taken in measured depth. Then, we interpolated the layer boundary depth to the depth of the EGRIP main core via 9 match points. We calculates annual means by averaging between annual layer boundaries of a 1 cm resolution. Further, we dated the ice core with the GICC05-EGRIP-1 EGRIP main core time scale and extrapolated the data above 23.9 m where no data of the main EGRIP ice core was available and below 122.58 m where the last match point was located. Additionally, we assumed that every layer boundary represents one year and added the missing gap of 6 m corresponding to a total age of 51 years. We calculates annual means by averaging between annual layer boundaries of a 1 cm resolution. The GICC05-EGRIP-1 timescale is based on the annual-layer-counted Greenland Ice Core Chronology from 2005. This Chronology relies on electrical conductivity measurement (ECM), measurements of chemical impurities, visual stratigraphy, dielectric profiling (DEP) measurements and tephra horizons of several ice cores (Rasmussen et al., 2013; Svensson et al., 2006; Vinther et al., 2006). Mojtabavi et al., 2019 transferred the GICC05 times scale from the North Greenland Ice Core Project (NGRIP) ice core supported by match points identified in the North Greenland Eemian (NEEM) ice core to the EGRIP main core. For more detail about the dating, please see Mojtabavi et al. (2019).

We only took the layer boundaries to be able to compute annual means, not to date the record (between 23.9 m and 122.58 m). It should be mentioned that there can be discrepancy between the age received from a segment in between the match points and the identified layer boundaries of a segment (Fig. 6). This discrepancy appears since we interpolated the layer boundary depth to the depth between the match points. We assumed that match points and depth of the layer boundaries are correct. Further, layer boundaries must be seen as pseudo annual layers since some layer intervals are too large or were not found by the StratiCounter algorithm for example due to missing data. Nevertheless, we considered this error to be small enough to be able to proceed with this age scale. Further work on the dating needs to be done to be able to accurately, absolutely date the ice core.

Figure 6 Off-set of the age scale from layer boundaries (in red) to consecutive years (in black). No layer boundary is found in between year 1647 to 1648 and 1649 to 1650 leading to a smaller number of years counted from layer boundaries compared to absolute years.

2.5 Statistical Analysis

Statistical summaries including mean, median, standard deviation, minimum and maximum concentration were made in addition to visual analysis of the time series to allow a descriptive overview of the data and its distribution. Additionally, we provided boxplots of the yearly mean values as well as histograms of the log-transformed data. All statistical analyses were conducted in the statistical software R (R Core Team, 2018).

2.5.1 Statistical Analysis of Extremes

Further, statistical analysis of extreme events in conductivity, Ca, Na, NO_3^- and NH_4^+ was conducted to examine their existence. With this, we wanted to look at their frequency and their relation to changes in boreal fire occurrences or atmospheric circulation anomalies due to e.g. volcanic eruptions, changes in storminess, or anthropogenic climate change. Extreme events are the part of the measured values that exceed a fixed threshold and cannot be explained by natural variability. To receive a robust threshold, which is able to identify extreme events, a statistical treatment needs to be conducted on the data set. We assume our background concentration to follow a theoretical log-normal distribution. Therefore, we took the logarithm of the annually averaged concentration for the statistical analysis of the data. Further

seasonal variability of the concentrations is filtered out by calculating yearly mean values. These calculations are like applying a low-pass filter to the dataset. As an initial approach, we followed Fischer et al. (2015) by using suitable time series analysis approaches. They investigated NH_4^+ extremes in the NGRIP and Greenland Ice Core Project (GRIP) record. Their threshold is a robust, non-sensitive measure for the background and its variability. We set the threshold following this work and calculated the running median (RM_i) of a specific window length (N).

$$RM_i = \text{median}(Y_i-(N-1)/2, ...,Y_i+(N-1)/2) \quad (4.1)$$

$$MAD_i = \text{median}(|Y_i-(N-1)/2 - RM_i|, ..., |Y_i+(N-1)/2 - RM_i|) \quad (4.2)$$

In this Master Thesis, the median of a 101-year moving window was chosen. We added the k times the running median of the mean absolute deviations (MAD_i). The factor k sets the position of the threshold. Those values Y at the time i exceeding this threshold

$$Y_i > RM_i + kMAD_i \text{ and } Y_i < RM_i + kMAD_i \text{ respectively for sodium} \quad (4.3)$$

were then the prospected outliers (extreme events).

2.5.2 Comparison with other Ice Cores

Additionally, we visually analysed the Na timeseries of the EGRIP S6 record and compared it to the timeseries of other shallow ice cores, namely Tunu and NEGIS. Tunu (78°3′N, 33°52′W, 213m) was drilled in 2013 and was located approximately 300 km northward of the EGRIP site (Maselli et al., 2017). The NEGIS firn core (75°38′N, 35°56′W, 67m) was drilled in 2012 and was located approximately 1 km eastward of the EGRIP site (Vallelonga et al., 2014). We had high resolution Na measurements for both cores, making it possible to compare the cores with the EGRIP S6 ice core. For Tunu an absolute age scale was available. For NEGIS we used match points and interpolated annual layers in between the match points to get to a rough age scale. To account for inaccuracy in absolute dating, we computed running means of an 11-year window.

2.5.3 Comparison with Atmospheric and Oceanic Circulation Patterns

We descriptively compared the NAO, PDO and AMO with the EGRIP S6 data. Additionally, we examined the linear relationships of the ice core record and the indices. For the comparison with the PDO and AMO, we used the running mean concentration of an 11-year window computed from the annual mean concentration of the EGRIP S6 layers. For the NAO, we compared the yearly mean concentration of our ice core record.

The annual NAO index covers the instrumental period from 1864 and is based on a pressure difference between stations on the Azores and Iceland. We took the annually resolved NAO Index provided by the Climate Analysis Section, NCAR, Boulder, USA. There are shortcomings using station-based NAO time series since the stations are fixed in space and might not provide a good representation of the

movement of the center of action of the NAO. Additionally, small-scale and transient meteorological phenomena that are unrelated to the NAO can add additional noise to the data. However, this index is a good representation of the NAO and is not based on a proxy reconstruction (Hurell, 2001). The PDO Index is defined as the first principal component of the North Pacific monthly sea surface temperature variability. The dataset is provided by NOAA/OAR/ESRL PSD, Boulder, Colorado, USA and closely follows the PDO index of Mantua & Hare (2002). The PDO index dates back to 1854. AMO is a measure of the North Atlantic sea surface temperature anomalies. We used two different AMO indices: a short time series based on instrumental data reaching back to 1856 based on the UK Met Office Kaplan sea surface temperature dataset. The long-term AMO reconstruction is provided by Mann et al. (2009) reaching back to 500 AD. It is based on documentary and natural proxies, mainly tree rings, where no instrumental data is available.

3 Results

In this section, we examine the long-term variability in the ice core record. Furthermore, we compare the S6 record with atmospheric circulation patterns and the Tunu and NEGIS sodium records.

3.1 Long-term Variation

In the following, we focus on the long-term variation by trend analysis and extreme value analysis. This is done to describe the aerosol record, its distribution and trend as well as to find extreme values and their frequency of occurrence.

3.1.1 Trend Analysis

Table 1 shows a statistical summary table of the measured components. As a second way to visualize the data, boxplots for annual means were created (Fig. 7). All data show outliers in the boxplots exceeding the upper whisker which is defined as 1.5 times the interquartile range above the third quartile. Conductivity has a mean value and a standard deviation of 1.32 ± 0.40 µS/cm over the last approximately 1000 years. We had to remove meter 20 to 26 from the nitrate data, since we changed the reagent in the measurement system leading to drift in the data. Therefore, we excluded the nitrate data in the time period from 1900 until 1933 AD from further analysis. Nitrate has a mean value and a standard deviation of 102.02 ± 38.88 ng/g. The average concentration and one standard deviation in sodium and calcium over the last approximately 1000 years amount to 10.16 ± 5.34 ng/g and 8.46 ± 5.34 ng/g respectively. The ammonium background signal drifts in the firn part of the ice core, which is located above the bubble close-off at around 67.39 m depth. This might be attributed to analytical problems caused by contamination from lab air. Therefore, we refrain from interpreting the long-term variations in the NH_4^+ concentration in this part of the ice core corresponding to the years 1600 to 2001 AD. The ammonium concentration for ages older than 1600 AD has a mean and a standard deviation value of 7.71 ± 10.92 ng/g. The high value of the standard deviation and the relatively low median (4.88 ng/g) need to be considered. The high variability in the concentration is attributed to the background concentration onto which high concentration peaks are superimposed. Nitrate and ammonium show the strongest variation and also appear to have more outliers than the other aerosol species.

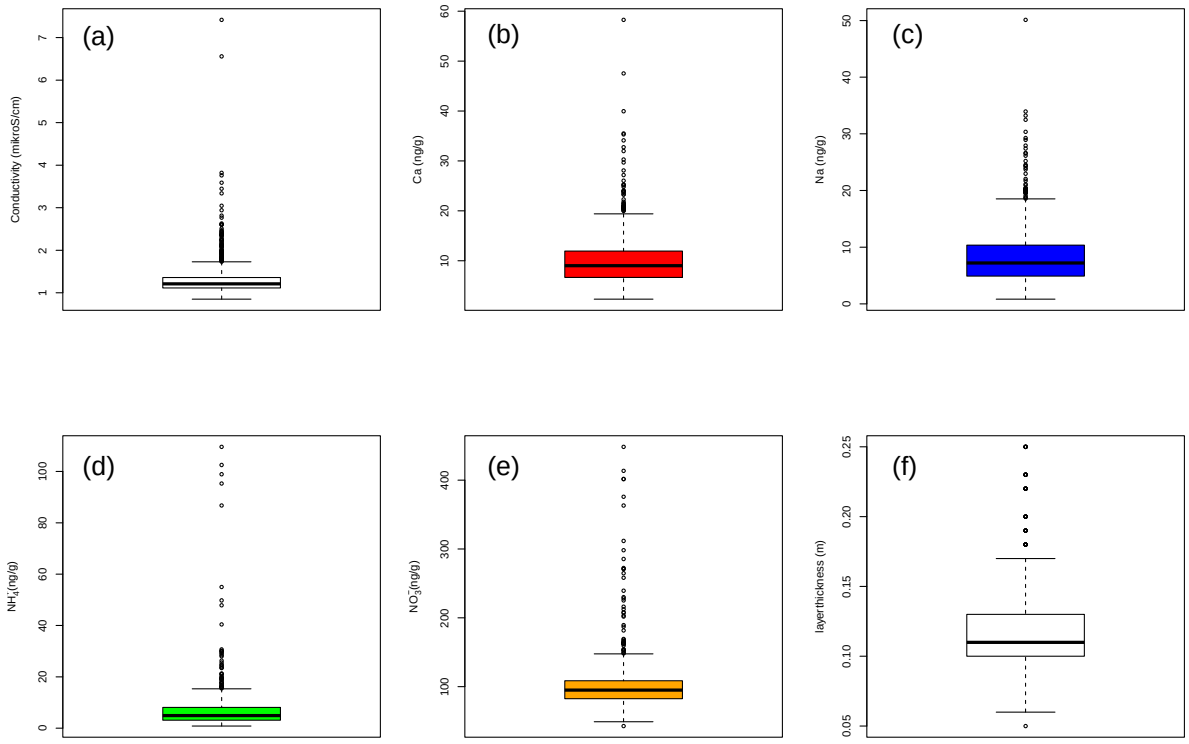

Figure 7 Boxplots of (a) conductivity, (b) calcium, (c) sodium, (d) ammonium (e), nitrate and (f) the layer thickness depicting outliers and skewness of the data with conductivity, ammonium and nitrate being skewed towards higher values. The box spans the first (lower horizontal line) to the third quartile (upper horizontal line) of the data with the median as the horizontal line (thicker line) in the box. This represents the interquartile range (IQR) showing 50% of the data. The lower whisker represents the first quartile minus 1.5×IQR and the upper whisker represents the third quartile plus 1.5×IQR. Outliers are all values (circles) that are either 1.5×IQR above the third quartile or 1.5×IQR below the first quartile. All variables show outliers exceeding the upper whisker and only nitrate and the layer thickness show one outlier exceeding the lower whisker.

Table 1 Summary table of aerosol components and annual layer thickness.

	Min. Value	1st Quartil	Median	Mean	3rd Quartil	Max. Value	Std. Deviation
σ (µS/cm)	0.85	1.13	1.21	1.32	1.36	7.42	0.40
Ca (ng/g)	2.31	6.66	9.00	8.46	11.94	58.26	5.34
Na (ng/g)	0.85	4.91	7.23	10.16	10.37	50.11	5.34
NH_4^+ (ng/g)	0.82	3.10	4.88	7.71	8.06	109.60	10.92
NO_3^- (ng/g)	42.79	82.91	95.54	102.02	108.63	448.41	38.88
λ (cm)	5.00	10.00	11.00	11.69	0.12	25.00	2.95

To be able to proceed with statistical testing, it is necessary to have normal distributed data. Probability density plots with underlying histograms are provided in Figure 8. The logarithm of calcium follows a normal, unimodal distribution. The logarithm of sodium is slightly skewed towards lower values compared to the normal

distribution. However, for the logarithm of conductivity, ammonium and nitrate the data is skewed towards higher values compared to the normal distribution. Conductivity and nitrate have a positive kurtosis indicating that its distribution has heavier tails than the normal distribution. The skew and kurtosis in the data is caused by additional exceptional events that are superimposed on the background distribution. However, it is assumed that their background distribution follow to a first order a log-normal distribution.

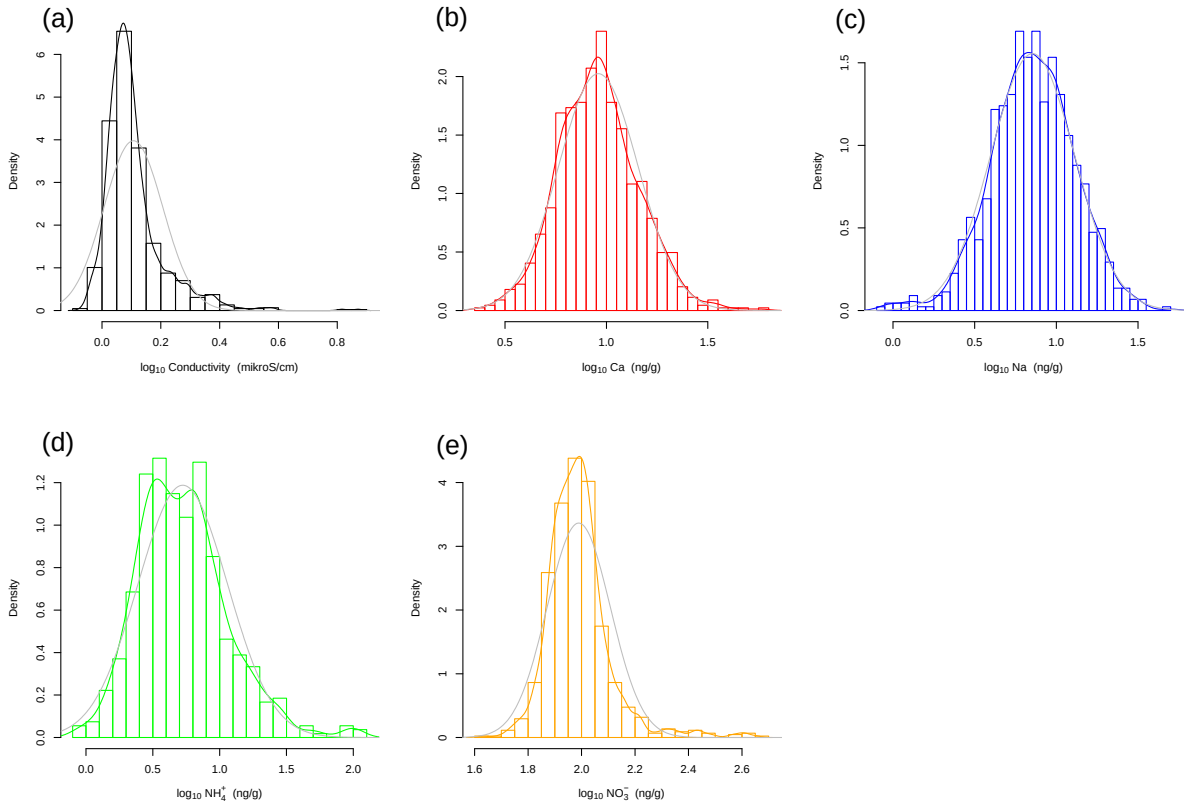

Figure 8 Probability density plots of the logarithm of the (a) conductivity, (b) calcium, (c) sodium, (d) ammonium and (e) nitrate concentrations with their normal distribution (grey) and their histograms (bar plot). Sodium is slightly skewed towards lower concentration and conductivity, ammonium and nitrate skewed towards higher values compared to the normal distribution.

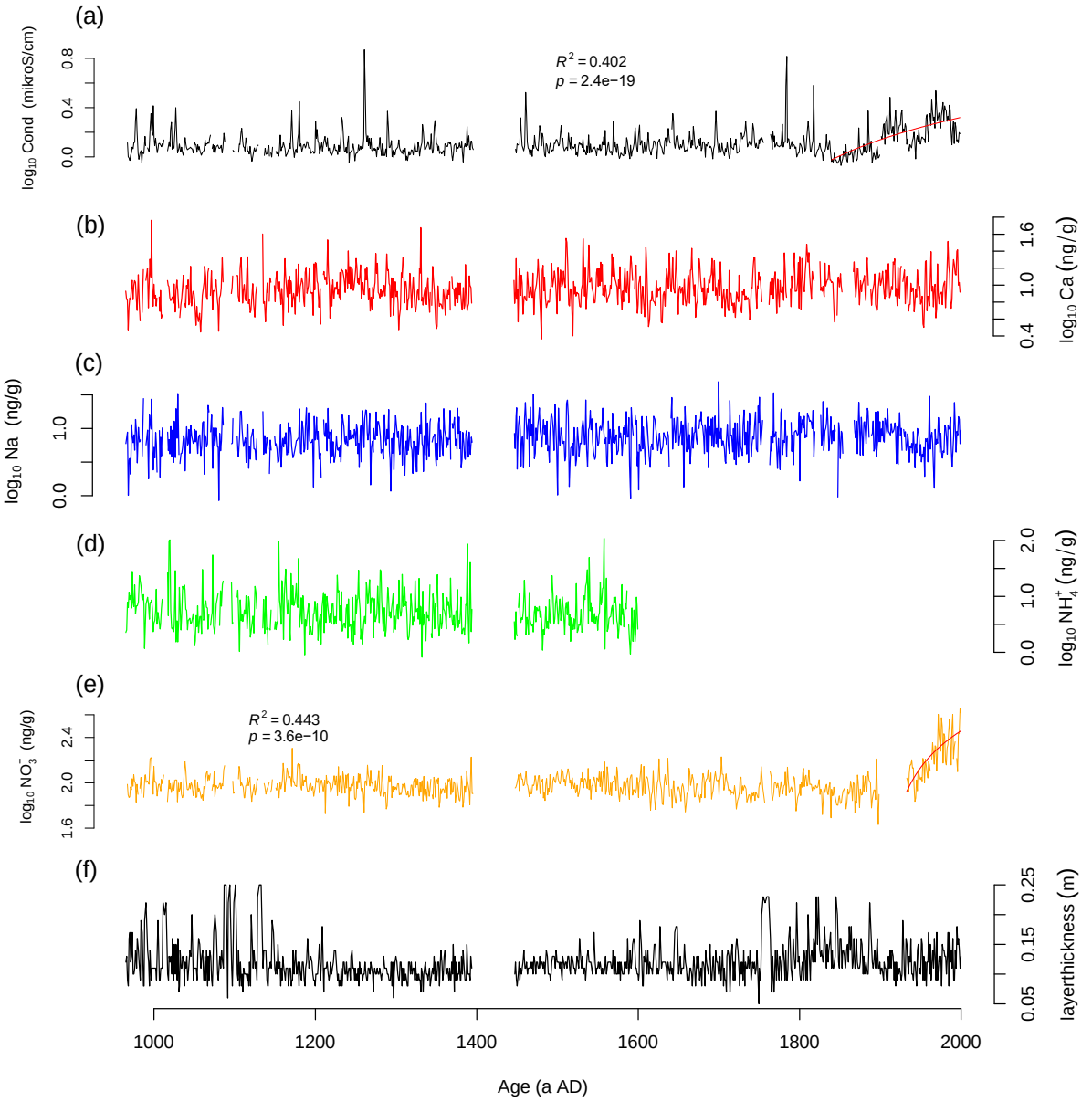

Figure 9 Logarithm of the annual (a) conductivity, (b) calcium, (c) sodium, (d) ammonium, (e) nitrate concentrations and (f) the annual layer thickness from 1030 to 2001 AD on a 1 cm resolution overlaid by the linear regression line (red) for the anthropogenic increase in conductivity and nitrate concentrations from 1840 to 2001 AD. The trend in conductivity and nitrate is calculated on the non-log transformed concentrations.

Figure 9 depicts the time series for annual conductivity and the annual calcium, sodium, ammonium and nitrate concentrations from 996 to 2001 AD. As Na, Ca and nitrate have high interannual noise, show less superimposed spikes and have no trend, only the background variation might be interesting to analyze. The sodium concentration seems to have more negative peaks than positive. For the trend analysis in conductivity we chose the period from 1840 to 2001 AD. For the trend analysis NO_3^- we chose the period from 1933 to 2001 AD after the data gap. Conductivity and NO_3^- concentration show a pronounced increase in this period, where most of the anthropogenic influence on NO_3^- and the conductivity, through anthropogenic emissions of NO_x, have taken place. Nitrate concentrations are 48.03 % and the

conductivity is 16.00 % higher in the industrialized period from 1933 to 2001 AD and from 1840 until 2001 AD respectively than in the time before. Linear regression was used to analyze the trend in concentration in this time span and determine at what rate NO_3^- and conductivity were changing. The density plot with a histogram of the residuals is provided in Figure 20 in the Appendix. The R^2 value for the conductivity is 0.40 (p = 2.4e-19) and for nitrate 0.44 (p = 3.6e-10). In each case, the R^2 value is rather high, indicating that the linear models explain a good part of the total variance. The model is significant under a level of significance of 5%. Nitrate concentrations increase strongly after the data gap from 1993 until 2001 AD. Until the end of the 20th century nitrate concentrations become more stable, however, the variability in NO_3^- increases. Conductivity shows two distinct peaks in the time strongly influenced by humans from 1840 until 2001. It increases from 1840 to 1910, then decreases until 1940, increases from 1940 onwards after it peaks during the 1980s and decreases until 2001 AD.

The mean annual layer thickness λ and one standard deviation is 11.68 ± 2.95 cm ice equivalent per year with higher levels from 950 to 1150 AD and from 1750 to 1870 AD (Fig. 9). This annual layer thickness is in line with the estimated annual layer thickness by Vallelonga et al. (2014). To be able to interpret variability in the accumulation rate a decadal layer thickness is needed. We calculated a smoothed layer thickness by a running mean of a 11-year window representing the decadal scale. The smoothed layer thickness displays long-term changes in snow accumulation rate, which can have an effect on all chemistry records. As can be observed in Figure 10, higher layer thickness is found from 1080 to 1170 AD and 1750 until 1900 AD. However, overall the mean annual accumulation rate shows only small variations over the last 1000 a. Since there is no trend in accumulation rate over the same period, we can assume that there is no effect on trends observed in conductivity and NO_3^-.

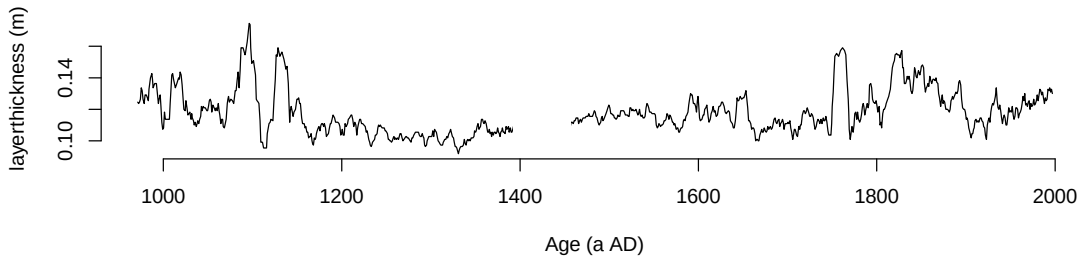

Figure 10 Layer thickness (m) calculated by a running mean of a 11-year window over the time period from 971 until 1997 AD for interpretation of the change in accumulation rate. Higher layer thickness is found from 1080 to 1170 AD and 1750 to 1900 AD. Higher layer thicknesses can be explained by data gaps in the annual layer count of the Straticounter algorithm.

3.1.2 Extreme Value Analysis

In extreme value analysis choosing a robust threshold is the most widespread approach in order to distinguish extreme events from background concentrations (e.g. Mudelsee, (2014)). When investigating extreme events, we account for double counting by eliminating values representing the same peak. Additionally, we accounted for all years without a value by linear interpolation between the values. We chose different values for the window length (N) and the threshold factor (k). N is set to 101-years since this is a good representation of the sample of a population in a statistical sense. Additionally, this can be considered a climatological relevant time period accounting for less short-term variability. Applying the running median method, we had to remove half of the window length at each side of the time series. These values are not reliable since the number of values to calculate the median was less than 50-years. This leaves us with a time period from 1022 to 1951 AD for the threshold calculation and from 1074 to 1901 AD for the frequency calculation of occurrence of extreme events. For ammonium we eliminated the time period after 1600 AD leaving us with a time period from 1022 to 1551 AD for the threshold calculation and from 1074 to 1500 AD for the frequency calculation of occurrence of extreme events. For nitrate we eliminated the time period after 1900 AD leaving us with a time period from 1022 to 1850 AD for the threshold calculation and from 1074 to 1800 AD for the frequency calculation of occurrence of extreme events. For the extreme value analysis we deleted the data gap from 86 to 92 m where no data was available. This was done in order to not shorten the length of the time series, which would have meant to remove half of the window length at each side of the time series for this period. Not to remove half of the window length at each side of the time series would lead to a threshold artefact and would therefore lead to an overestimation of the frequency of occurrence of extreme events. Figure 11 depicts this problem.

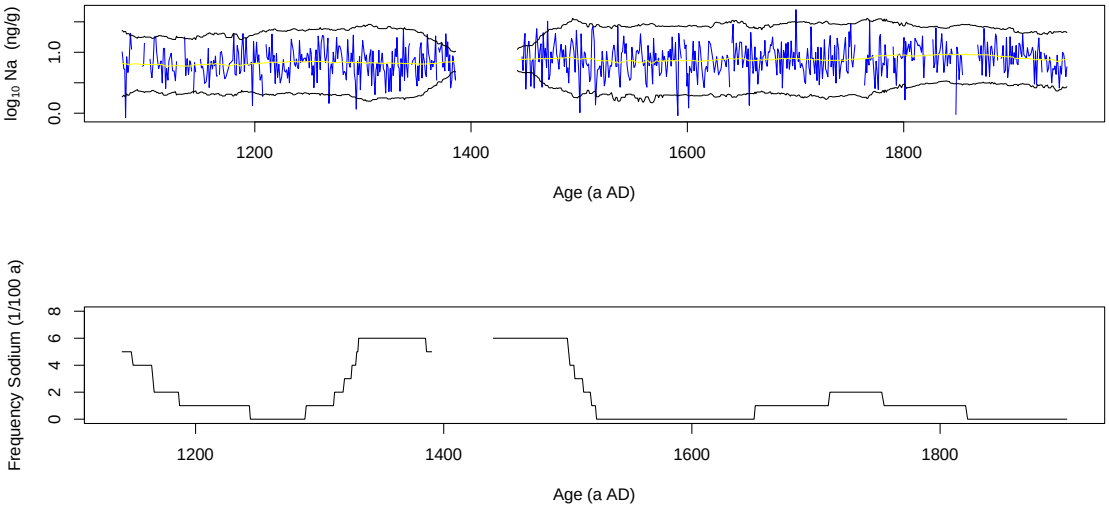

Figure 11 The graphs depict the logarithm of the annual (a) sodium concentrations from 1022 to 1951 AD and (b) the frequency of the sodium record from 1074 to 1901 AD. The sodium concentrations are overlaid by the running median (RM_i) of a 101 year window (yellow) and a factor k times the median absolute deviation (MAD_i) of the same window length added to/subtracted from the running median (RM_i) (black) representing the upper and lower threshold. The frequency plot depicts the counts of extreme values computed by the total sum of counts in a 100-year window. As clearly illustrated in this figure, including the years with missing values during the data gap would lead to an overestimation of extreme events found by the threshold during the time around the data gap which is also depicted by an overestimation of the frequency of occurrence of extreme events during this time period.

In the extreme value analysis, we did not interpolate for missing values. Therefore, we cannot make assumptions about extreme events for years with missing data. However, we interpolated missing data for the threshold calculations since this was a prerequisite for the running median and absolute median deviation function in R (R Core Team, 2018).

With our method, we look at the overall picture from source emissions to transport and deposition effects. However, we cannot assume completeness of the ice core time series to record each individual event, since they are highly dependent on air-mass transport. However, we can make assumptions of the relative change of extreme events in a sufficiently long time span. With this method, we get a reliable picture of the mean change in frequency distribution. Therefore, we provide a robust estimate on the general extreme event occurrence. We are interested in extremely high concentrations in the aerosols and low concentrations for sodium. Therefore, we need to set a threshold to retrieve extreme events. Not to over- or underestimate the extreme events, we chose to set a symmetric threshold. The upper threshold is defined by setting the lower threshold and vice versa for sodium. This threshold is set in a way that 5% of the observations exceed this lower threshold and the upper threshold for sodium. Therefore, we chose the factor k such that 5% of the lower concentrations are below this threshold. This approach accounts for the natural variability in the data and does not under- or overestimate the number of extreme events. This leads to 9 outliers for component for the lower threshold and 5 outliers for the shorter ammonium time

series (Tab. 2). For sodium this leads to 9 outliers for the upper threshold (Tab. 2). The k value for every component can be found in Table 2. Those values exceeding the upper threshold (lower threshold for sodium) are considered extreme events. Figure 12 shows the long-term conductivity and aerosol concentrations from 1022 to 1951 AD, 1022 AD to 1551 AD for ammonium and 1022 to 1850 AD for nitrate overlaid by the running median (RM_i) of a 101-year window and a factor times the median absolute deviation (MAD_i) of the same window length added to/subtracted from the RM_i. Table 2 shows the resulting total sum of extreme events exceeding the threshold.

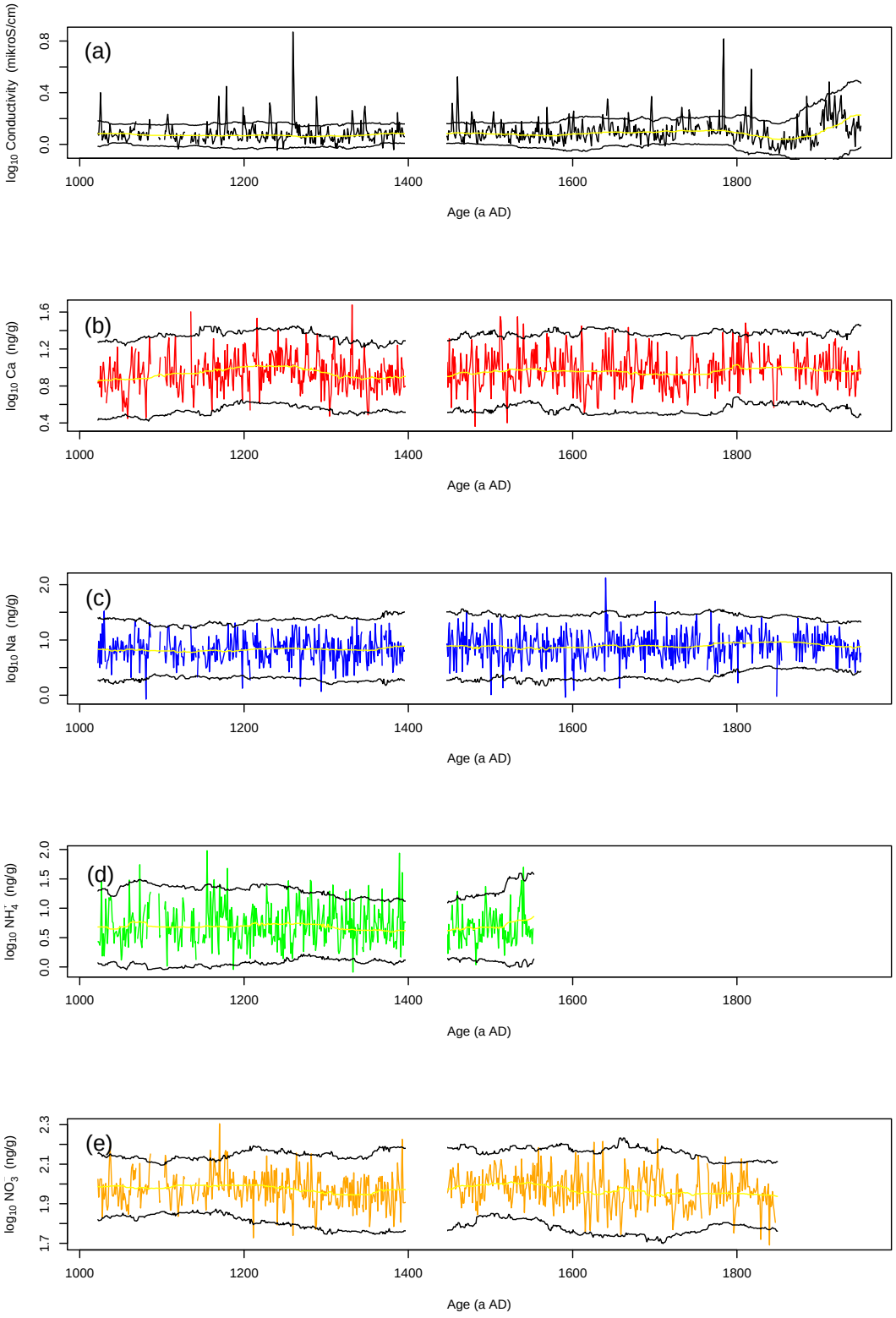

Figure 12 The graphs depict the logarithm of the annual (a) conductivity and (b) calcium, (c) sodium, (d) ammonium and (e) nitrate concentrations from 1022 to 1951 AD and 1022 to 1551 AD for ammonium overlaid by the running median (RM_i) of a 101 year window (yellow) and a factor k times the median absolute deviation (MAD_i) of the same window length added to/subtracted from the running median (RM_i) (black) representing the upper and lower threshold. Values exceeding this threshold represent extreme values.

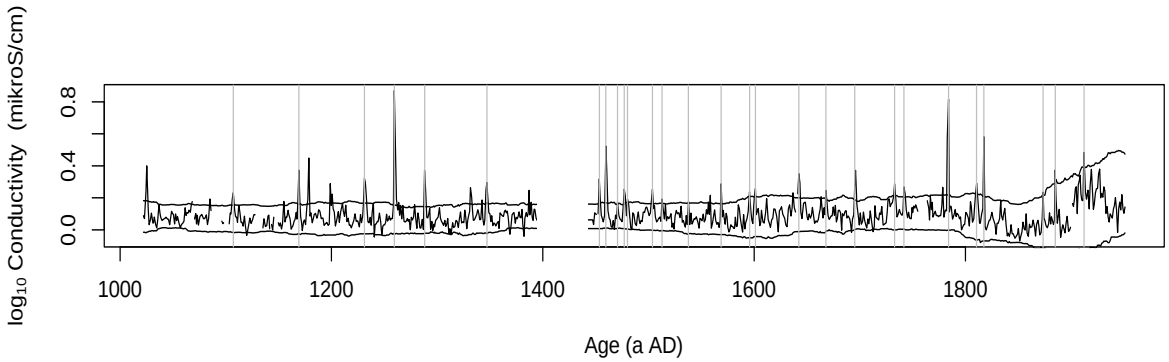

Figure 13 The figure shows the threshold method applied to the conductivity record. Shown are historical volcano eruptions (grey) detected by the upper threshold underlaid by the upper and lower threshold and the conductivity record during the time period from 1022 until 1951 AD.

We validated this approach by checking for major historical volcanic eruptions presented in the ice core record (Fig. 13). For this analysis, we took the conductivity which is a bulk parameter. To a large extent it is influenced by sulfuric acid concentrations which in turn represent volcanic eruptions. These historic volcanic eruptions as well as the dating and the dating error can be found in Table 3 of the Appendix. With our approach, we found 28 major peaks that were attributed to historical volcanic eruptions in Sigl et al. (2013) and the year of the eruption also matched the year of occurrence in the ice core record with an error of ±1 years. The small error of ±1 years also confirms our dating approach.

Table 2 Number of extreme events exceeding the threshold of conductivity, calcium, sodium, ammonium and nitrate with their specific threshold factor k which determines the position of the threshold.

	σ (µS/cm)	Na (ng/g)	Ca (ng/g)	NH_4^+ (ng/g)	NO_3^- (ng/g)
threshold factor k	1.96	2.22	2.30	2.00	2.87
# extreme events	52	12	13	24	9
# counts lower threshold	9	9	9	5	9
# of doublecounts upper threshold	23	2	1	1	0
# of doublecounts lower threshold	0	0	0	0	1

In a second step, the number of peaks per year in a running window of 101-years was counted. If one peak was depicted in several successive years, we only counted it as one extreme event. The frequency of occurrence of extreme events and the corresponding error is depicted in Figure 14. The occurrence of extreme events ought to follow a Poisson distribution. Therefore, its error is defined as the square root of the number of counts. Conductivity shows high occurrence of extreme values from 1210 until 1310 AD with its maximum of 13 ± 3 extreme events and from 1450 until

1500 AD and comparatively fewer extreme values from 1500 AD onwards. On average 7 ± 3 extreme events per century for conductivity and 5 ± 2 extreme events per century for ammonium were found. The calcium record indicates that a higher frequency of extremes occurred particularly at the transition from 1480 to 1530 AD. Sodium is relatively stable showing more extreme events from 1040 until 1180 and from 1310 until 1520 AD. Calcium and sodium have high interannual noise and only a small number of extremes could be identified. The ammonium frequency is highest from 1110 to 1350 AD. As mentioned before, the kurtosis of the ammonium data and the high maximum values relate to exceptionally high concentration peaks (Tab. 1), which can also be seen in the time series plots (Fig. 8) leading to a maximum value of 10 ± 3 extreme events in a century. Nitrate extreme value occurrence shows one distinct peak from 1140 until 1230 AD with its maximum value of extreme events of 4 ± 2. It needs to be mentioned that the occurrence of extreme values is generally very low except for conductivity which is a bulk parameter and cannot be separately interpreted in terms of source region, transport pathways and depicts mostly volcanoes in the extremes. The mean value of occurrence of an extreme event during the time period is 1 ± 1 extreme event per century for sodium and 2 ± 1 extreme events per century for calcium and nitrate. The maximum value for calcium and sodium is 4 ± 2 extreme events occurring per century. In light of the small number of identified extreme events, a comparison to atmospheric circulation patterns is not attempted Therefore, we proceed with a direct correlation of the ocean/atmospheric indices representing atmospheric circulation pattern with the aerosol concentration.

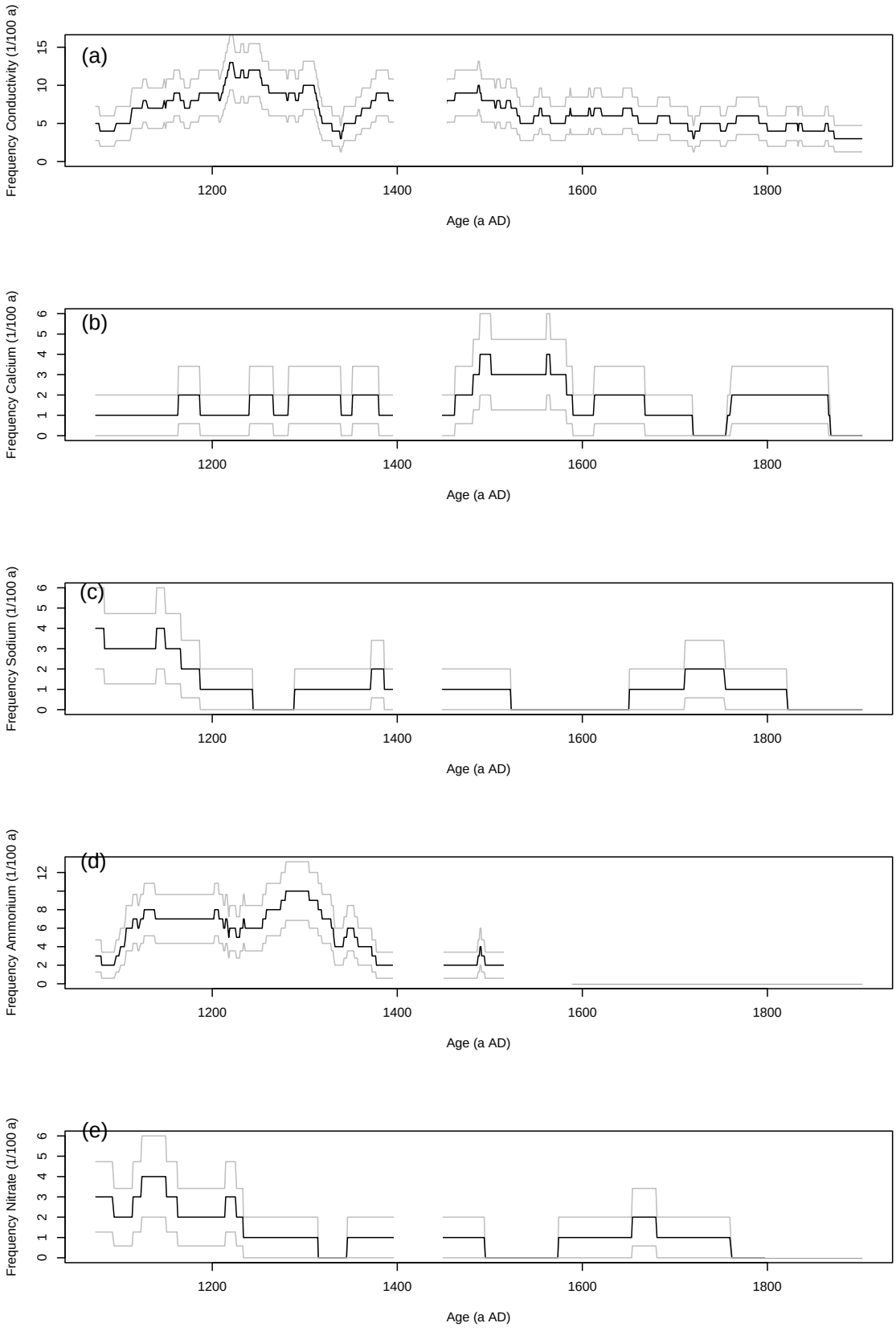

Figure 15 Frequency plots of (a) conductivity (b) calcium, (c) sodium, (d) ammonium and (e) nitrate depicting the counts of extreme values from 1074 to 1901 AD computed by the total sum of counts in a 100-year window. The error is depicted with a grey line computed by the √counts.

3.2 Decadal to Interannual Variation

In this section, we determine the linear relationship of the EGRIP S6 ice core record to the sodium record of the Tunu and NEGIS ice core as well as to oceanic and atmospheric indices by correlation analysis.

3.2.2 Correlation of Tunu, EGRIP S6 and NEGIS Sodium Record

We correlated the sodium concentration of the NEGIS, EGRIP S6 and Tunu ice cores calculated by the running mean filter with a bandwidth of 11 years. This provided us with a time series without data gaps since the data was interpolated where missing values occurred. The smoothing was needed to correct for the NEGIS age scale since it was not done with an annual layer count. To account for autocorrelation in the smoothed data, we corrected the p-value with a conservative, reduced number of degrees of freedom. The degrees of freedom are calculated by the effective number of datapoints (n_{eff}) which is the number of datapoints divided by the window length of 11-years. Applying the running mean method, we had to remove half of the window length at each side of the time series. We interpolated the data to the EGRIP S6 age scale and interpolated missing data for the threshold calculations since this was a prerequisite for the running mean function in R (R Core Team, 2018). Figure 15 depicts the sodium records of the three different ice cores.

The analysis is restricted to the interval from 1640 to 2001 AD due to the fact that the NEGIS record ranges from 1640 to 2012 AD and the EGRIP S6 record from 966 to 2001 AD. The correlation coefficient between Tunu and NEGIS is 0.37 ($p = 0.0503$, $n_{eff} = 30.45$), between Tunu and EGRIP S6 is 0.33 ($p = 0.0733$, $n_{eff} = 30.45$) and between NEGIS and EGRIP S6 is 0.06 ($p= 0.6323$, $n_{eff} = 30.45$). Only the correlation between the Tunu and EGRIP ice cores and Tunu and NEGIS ice cores, however, is statistically significant on the 10% level but not statistically significant on the 5% level. The mean and one standard deviation for the sodium concentration of the three ice core sites is 24.71607 ± 3.489447 ng/g for NEGIS, 13.8584 ± 9.283886 ng/g for Tunu and 9.17786 ± 5.63623 ng/g for EGRIP S6.

For the Tunu and EGRIP S6 sodium concentrations measurements an ICP-MS system was used (Erhardt et al., 2019; McConnell et al., 2002). NEGIS sodium concentrations reveals generally a higher baseline (about twice as high) as the Tunu and EGRIP S6 sodium records. The NEGIS sodium concentration was measured with a CFA system measuring the sodium ion concentration (Vallelonga et al., 2014). This could be a possible explanation for the higher sodium concentrations. The accumulation rate of the NEGIS ice core could not be calculated, since the provided dataset has no annual layer count. Furthermore, the provided dataset of the Tunu ice core has no layer depth. Therefore, we are not able to calculate the layer thickness and make further assumptions about the accumulation rate. Maselli et al. (2017), however, estimated it to be 11 cm per year. This is the same amount as calculated for NEGIS and EGRIP S6 (Vallelonga et al., 2014).

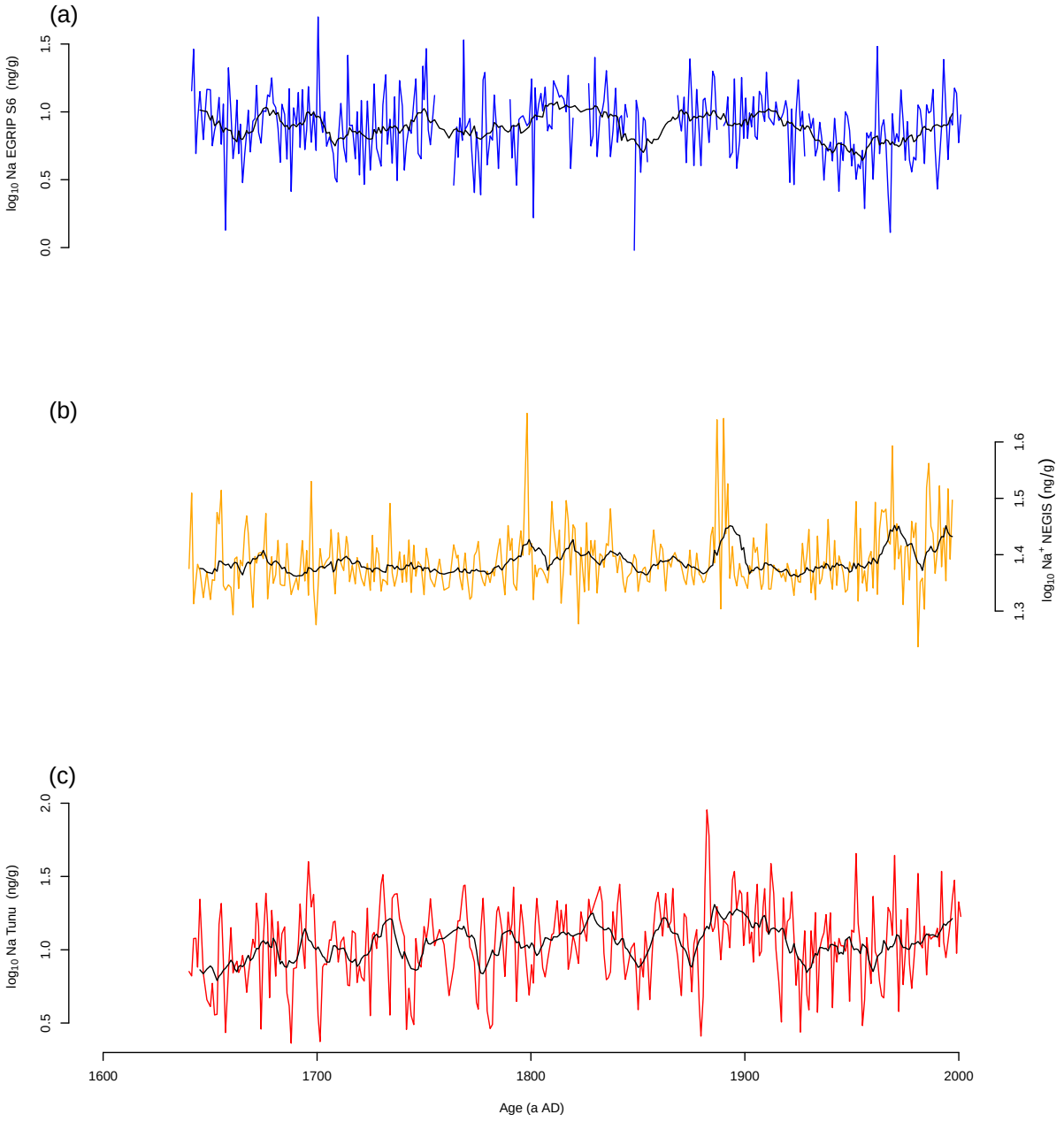

Figure 15 Annual sodium concentrations of the time period from 1640 to 2001 AD from EGRIP S6 (top), Tunu (middle) and NEGIS (bottom) overlaid by the sodium concentration calculated with a running mean of a 11-year window (black lines).

3.2.1 Correlation of the Ice Core Record with the AMO, NAO and PDO Index

In the following, we focus on the linear correlation of atmospheric as well as oceanic indices to be able to interpret the influence on the ice core record. We excluded the conductivity from the further analysis since it shows multifactorial influences and is therefore difficult to interpret. Ammonium is only correlated with the long AMO index before 1600. We excluded the data gap from 1395 to 1446 AD from the calculations and remove half of the window length at each side of the data gap. For nitrate, we excluded the data gap from 1900 to 1932 AD from the calculations and remove half of

the window length at each side of the data gap. We interpolated the data to the EGRIP S6 age scale where necessary and interpolated missing data for the threshold calculations since this was a prerequisite for the running mean function in R (R Core Team, 2018). We chose the level of significance α to be 5 %. For the AMO indices and the PDO index correlation, we smoothed the data by using a running mean of an 11-year window. This provided us with a time series without data gaps for the AMO indices and the PDO index since the data was interpolated where missing values occurred. For the NAO and the data gap in the long AMO calculations, missing data was excluded from the correlation calculations. This leads to 132 degrees of freedom for calcium and sodium and 116 degrees of freedom for the calculation for the p-value calculation of nitrate and NAO index. To account for autocorrelation in the smoothed data, we corrected the p-value with a conservative, reduced number of degrees of freedom. The degrees of freedom are calculated by the effective number of data points (n_{eff}) provided in Table 4-6 which is the number of data points divided by the window length which is 11-years. Applying the running mean method, we had to remove half of the window length at each side of the time series. The indices are plotted along with the aerosol record in Figure 16-19.

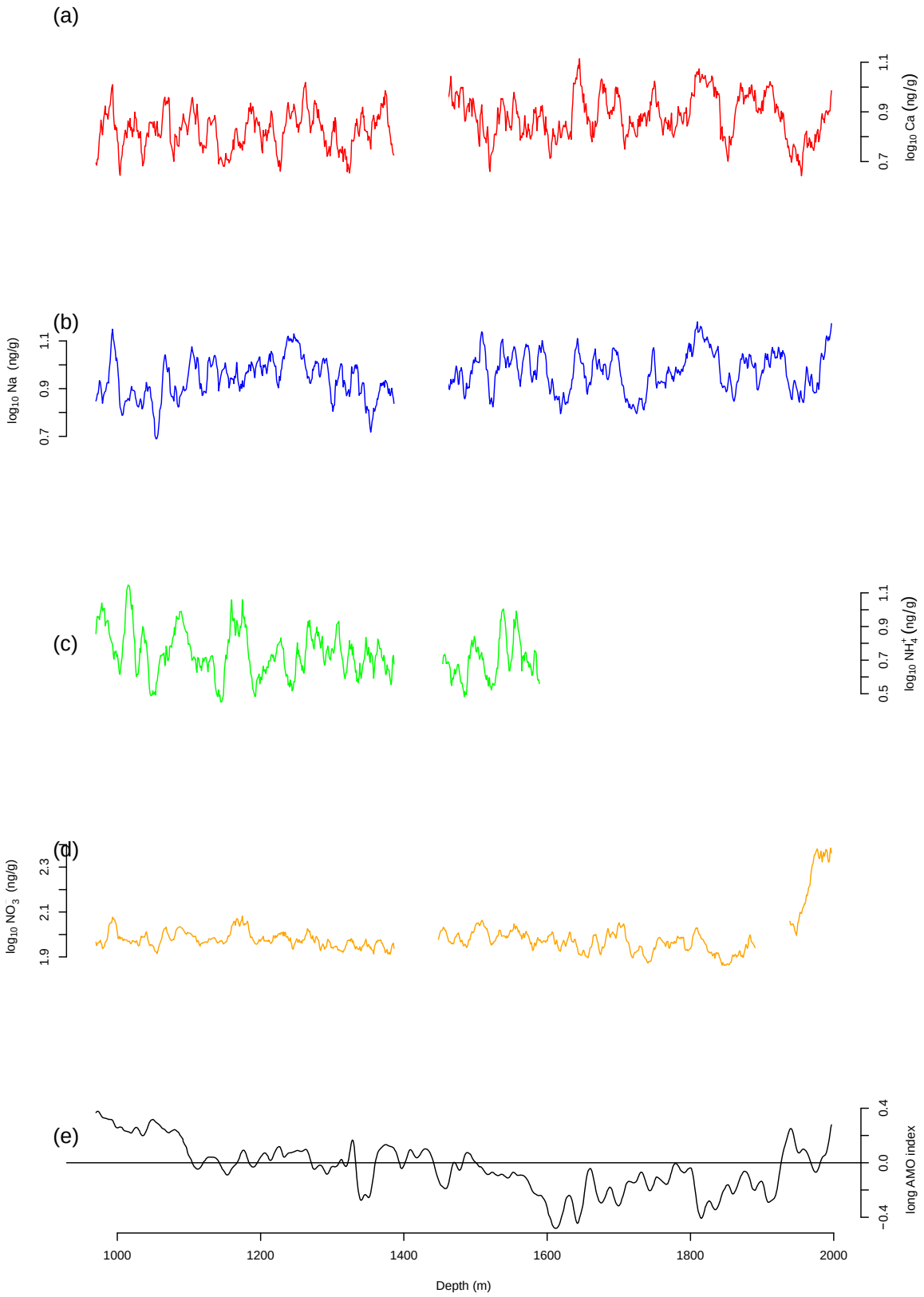

Figure 16 Logarithmic (a) calcium, (b) sodium, (c) ammonium and (d) nitrate concentrations and the (e) AMO index calculated by a running mean of an 11-year window over the time period from 975 until 1996 AD and 975 to 1595 AD for Ammonium. Values above the horizontal line in the AMO represent the positive phase of the AMO and values below the horizontal line represent the negative phase of the AMO.

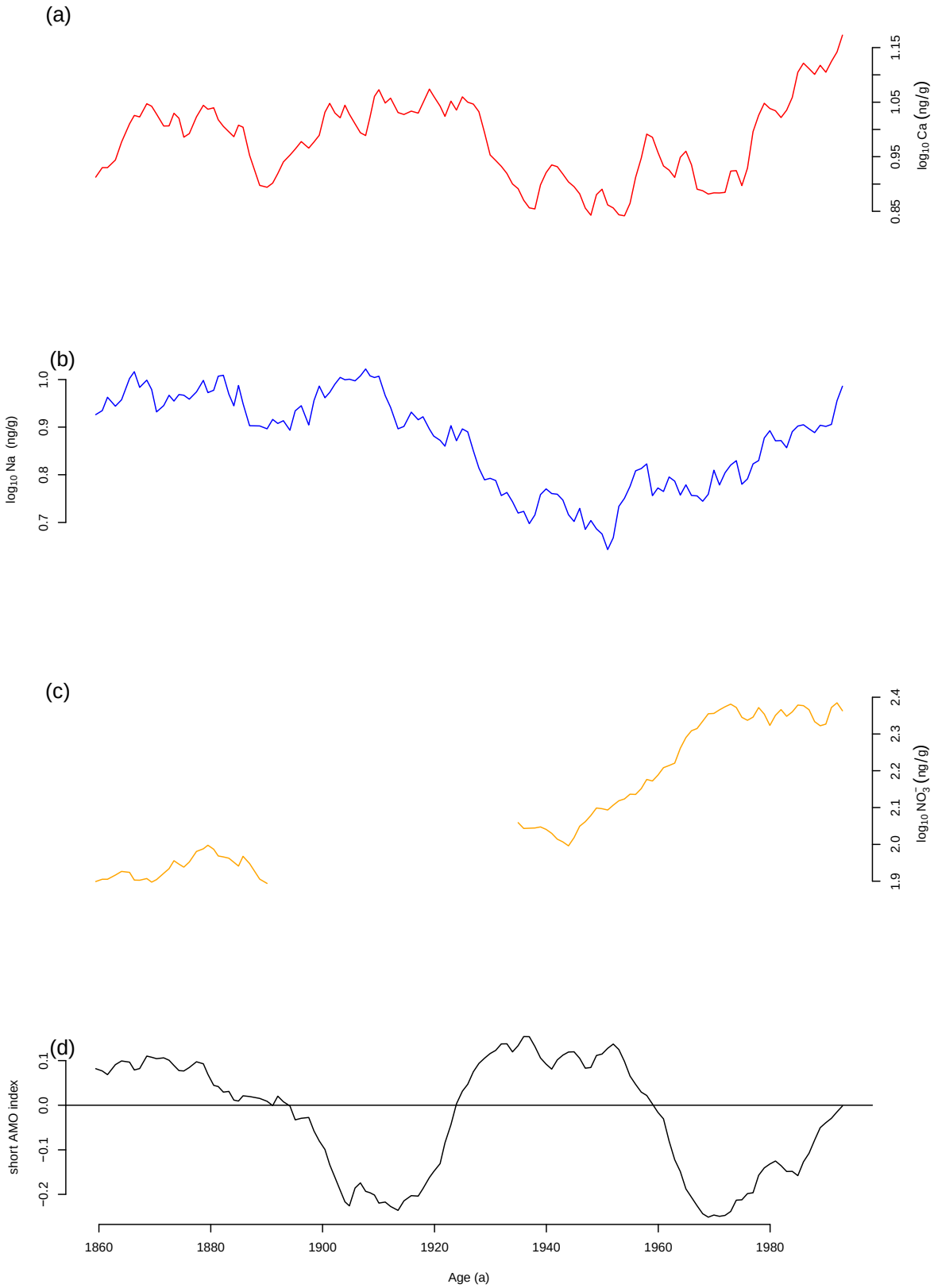

Figure 17 Logarithmic (a) calcium, (b) sodium, (c) nitrate concentrations and the (d) AMO index calculated by a running mean of an 11-year window over the time period from 1861 until 1996 AD. Values above the horizontal line in the AMO represent the positive phase of the AMO and values below the horizontal line represent the negative phase of the AMO.

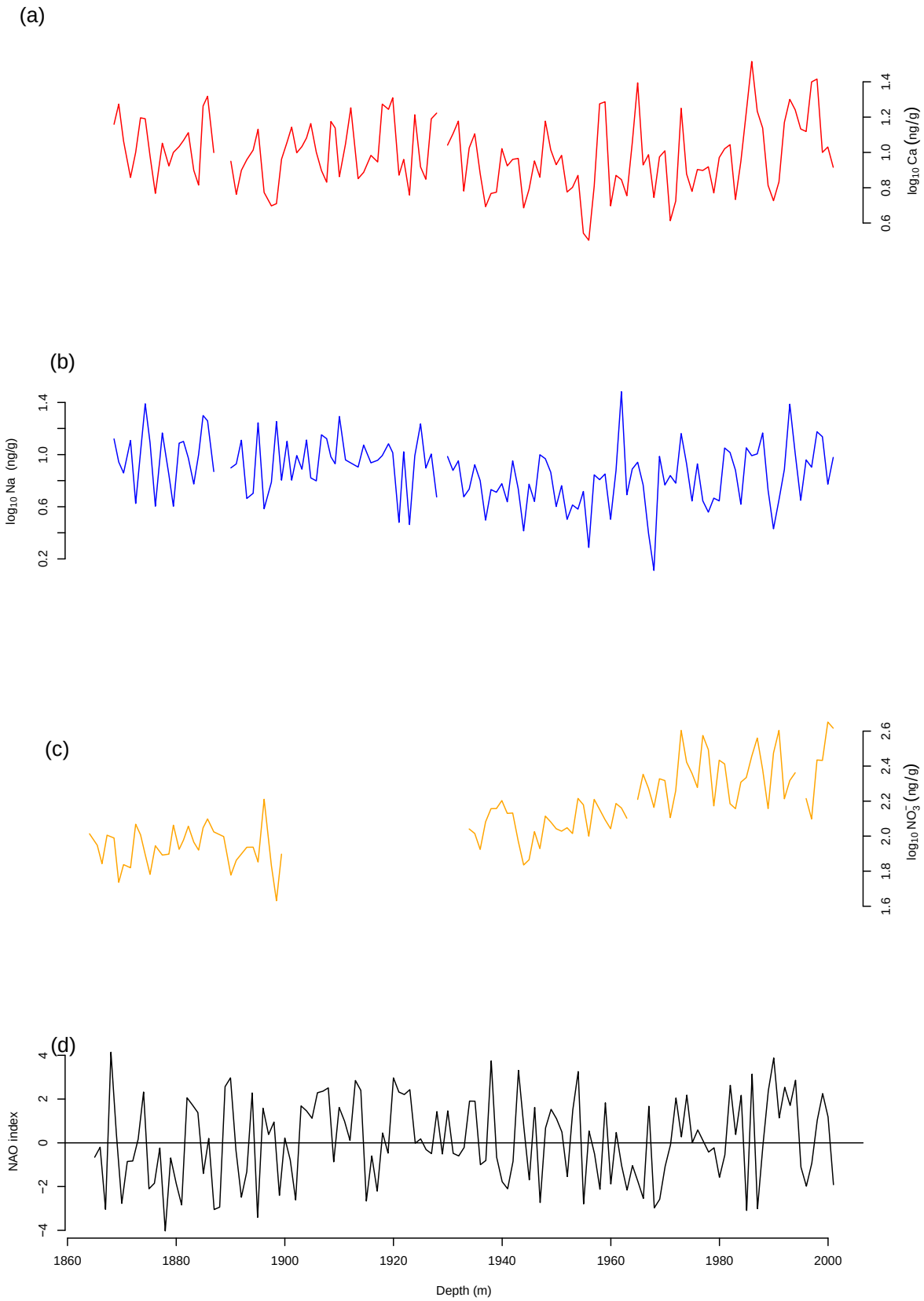

Figure 18 Logarithmic (a) calcium, (b) sodium, (c) nitrate concentrations and the (d) NAO index on an interannual time scale from 1864 until 2001 AD. Values above the horizontal line in the NAO represent the positive phase of the NAO and values below the horizontal line represent the negative phase of the NAO.

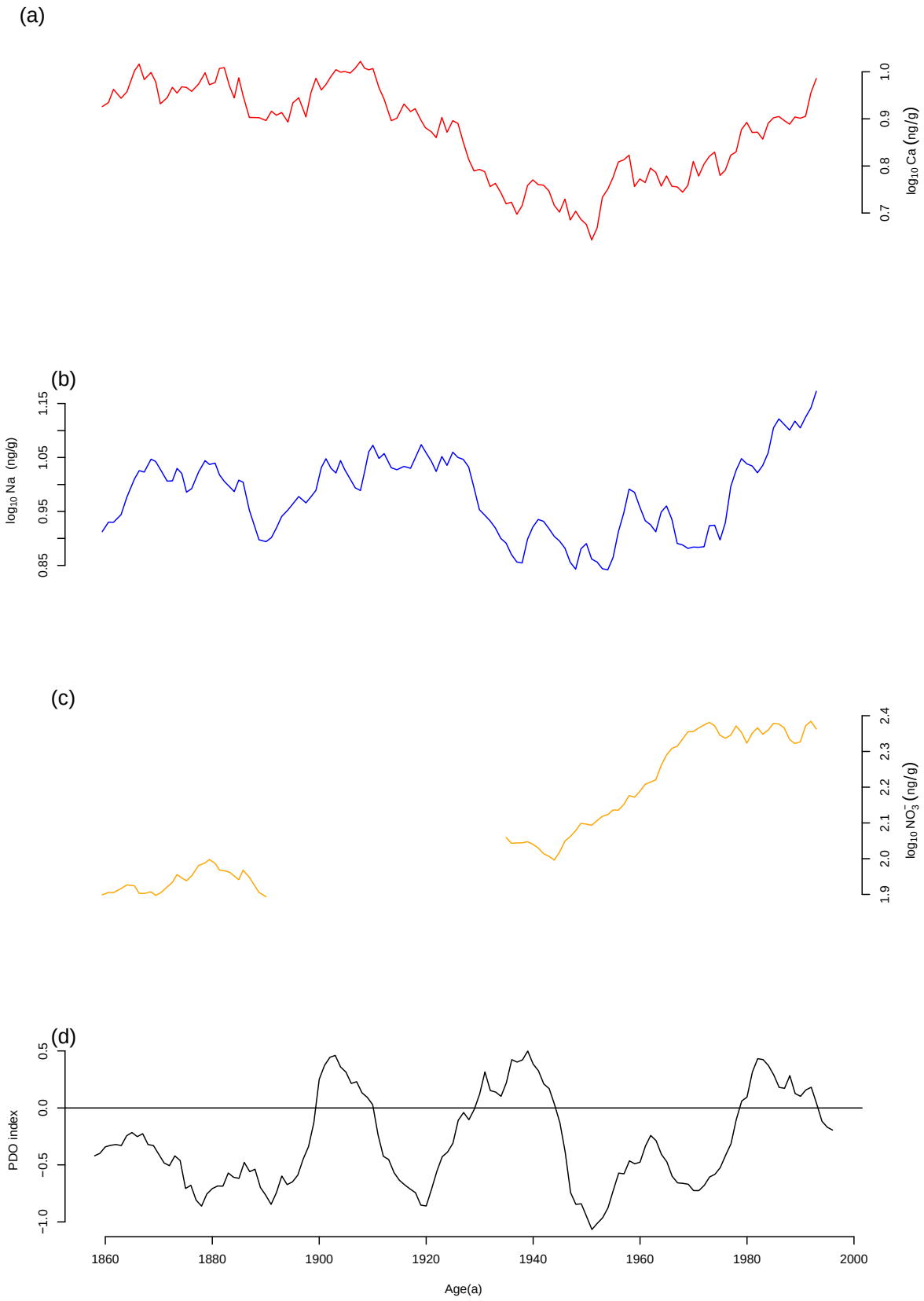

Figure 19 Logarithmic (a) calcium, (b) sodium, (c) nitrate concentrations and the (d) PDO index calculated by a running mean of an 11-year window over the time period from 1859 until 1996 AD. Values above the horizontal line in the AMO represent the positive phase of the PDO and values below the horizontal line represent the negative phase of the PDO.

The AMO is a measure of North Atlantic sea surface temperature anomalies. We used two AMO indices: A long AMO reconstruction from 500 to 2001 AD and a short station based AMO index from 1856 to 2001 AD (Mann et al., 2009). We used the AMO index starting from year 970 AD since the long AMO reconstruction dates further back than our ice core record. For the long AMO index calcium and sodium are significantly correlated on a 5% significance level (Tab. 3;4). Calcium and sodium are negatively correlated with the long AMO index and short AMO index. The calcium and nitrate correlations are rather high for the long AMO index with -0.24 for calcium, -0.37 for sodium. Nitrate is negatively correlated with the short AMO but positively correlated with the long AMO index. Interestingly, it is only significantly correlated with the short AMO index on a 5% significance level (Tab. 3). The correlation is generally low for indices on an interannual timescale. The NAO is a measure for pressure difference between stations on the Azores and Iceland (Hurell, 2001). No significant correlation is found between the PDO index and the calcium, sodium and nitrate record (Tab. 5).The PDO is a measure for SST anomalies over the northern Pacific Ocean on a decadal scale (Mantua & Hare, 2002). No significant correlation is found between the PDO index and the calcium, sodium and nitrate record (Tab. 6).

Table 3 Correlation coefficient and p value of the correlation of a running mean of an 11-year window of the short AMO index and the logarithmic calcium, sodium and nitrate concentrations and the effective number of data points (n_{eff}).

N_{eff} Ca; Na = 12.37 N_{eff} NO_3^- = 8.45	Ca (ng/g)	Na (ng/g)	NO_3^- (ng/g)
p value	0.3038	0.4703	0.0057
correlation coefficient	-0.31	-0.22	-0.82

Table 4 Correlation coefficient and p value of the correlation of a running mean of a 11-year window of the long AMO index and the logarithmic calcium, sodium, ammonium and nitrate concentrations and the effective number of data points (n_{eff}).

N_{eff} Ca; Na = 83.09 N_{eff} NH_4^+ = 48.54 N_{eff} NO_3^- = 78.64	Ca (ng/g)	Na (ng/g)	NH_4^+ (ng/g)	NO_3^- (ng/g)
p value	0.0308	0.0006	0.1024	0.0969
correlation coefficient	-0.24	-0.37	0.24	0.19

Table 5 Correlation coefficient and p value of the correlation of the NAO index and logarithmic calcium, sodium and nitrate concentration.

	Ca (ng/g)	Na (ng/g)	NO_3^- (ng/g)
p value	0.8109	0.2052	0.0663
correlation coefficient	0.02	-0.11	0.15

Table 6 Correlation coefficient and p value of the correlation of a running mean of a 11-year window of the PDO index and the logarithmic calcium, sodium and nitrate concentrations and the effective number of data points (n_{eff}).

N_{eff} Ca; Na = 12.55 N_{eff} NO_3^- = 8.64	Ca (ng/g)	Na (ng/g)	NO_3^- (ng/g)
p value	0.4321	0.8890	0.3185
correlation coefficient	0.24	0.04	0.38

4 Discussion

In this section, the results of the trend analysis as well as the extreme value analysis are discussed. Further, we focus on the discussion of the correlation of the sodium record of the Tunu and NEGIS ice cores with the EGRIP S6 ice core sodium record and of the EGRIP S6 ice core record with atmospheric and oceanic indices.

4.1 Trend Analysis and Extreme Value Analysis

Our trend analysis depicts an increase in conductivity and nitrate concentration. We found a decrease in conductivity starting in the 1980s AD onwards and a dip around 1940 AD. Our accumulation rate stays relatively stable over time. Therefore, the trend in nitrate and conductivity is not attributed to changes in the annual layer thickness. Since no distinct change of the source region is expected, a trend in aerosol concentration can be attributed to aerosol emissions caused by human activities. During the North Greenland Traverse (NGT) several shallow ice cores were drilled. Their nitrate and sulfate records show an increase during the 20th century (Fischer et al., 1998a). Fischer et al., (1998b) attributed industrial and vehicle emission from Europe and North America to this increase. Our trend analysis also depicts an increase in conductivity and nitrate concentration, which we can attributed to anthropogenic emissions depicted in the EGRIP S6 ice core. The trend in conductivity is caused by nitrate and sulfuric acid emissions. Fischer et al., (1998b) attributed the dip in conductivity to fewer anthropogenic emissions during the 1930s and may also be attributed to lower emissions during and slightly after World War II. The modern decrease in conductivity may be caused by a decline in industrial production in the former USSR starting in the 1970s and effective measures against sulfur emission in Europe and the United States (Fischer et al., 1998b). Nitrate concentrations increase strongly after the data gap from 1933 until around 1980 AD. The nitrate concentration is relatively stable from 1980 until 2001 AD. Additionally, there is a variability in NO_3^- increases until the end of the 20th century. This might be explained by the anthropogenic emissions leading to a more variable concentration measured in the upper meters of the core. The calcium, sodium and ammonium record depict high interannual variability but no overall trend. Therefore, changes in the source emission or anthropogenic influences can be excluded.

Conductivity and ammonium show high concentration peaks relative to the background concentration related to the occurrence of a few but distinct extreme events. The same holds for a few distinct low concentration peaks in sodium. These peaks are further analyzed in the extreme value analysis. The skewness in the conductivity is mainly caused by extreme events coming from sulfuric acid of volcanic eruptions which are confirmed by detection of historical volcanic eruptions in the extreme value analysis. The positive skew in ammonium is caused by additional exceptional biomass burning events that are superimposed on the background distribution which consists of emissions of biogenic activity in soil and in the surface ocean. We excluded the ammonium data from 1600 to 2001 AD since we had an unexplained trend in the data before the bubble close off. We attributed this to

contamination during the measurements. This unexplained trend in ammonium needs further attention but will not be discussed in this Master thesis. Sodium is a tracer for sea salt which is mostly transported from its source region by cyclones to Greenland (Rhodes et al., 2018). The skew in the sodium concentration might not be caused by dilution effects during relatively strong precipitation events since the extreme events do not coincide with high layer thicknesses. However, scavenging en-route may be most important diluting the sodium aerosol during the transport pathway.

We examined the annual layer thickness over an 11-year window in order to be able to make assumption about the accumulation rate, which is a good estimate for decadal changes in precipitation. Variations in the accumulation rate can change the aerosol concentration in the ice. These variations are determined by changes in the annual layer thickness that might be attributed to changes in wet deposition (Fuhrer et al., 1993). Vallelonga et al., (2014) found surface undulations in the vicinity of the NEGIS drill site. They attributed variations in accumulation rate to flow related changes in the surface topography due to bed topography. This surface topography will function as a snow trap which does not change its spatial position. Since the ice stream is moving, this will lead to a short term change in accumulation rate (Gow, 1965). Additionally, high values in the layer thickness relate to missing data since the Straticounter algorithm does not perform well where data gaps exist, leading to a higher annual layer thickness. Note that the annual layer thickness gives no information about changes in seasonal accumulation. Changes in seasonal accumulation would also have an effect on the aerosol concentration since the maximum concentration of the aerosols are deposited during a preferred season.

We conducted extreme value analysis in order to detect positive or negative outliers and their frequency of occurrence in an ice core record. For the detection of the extreme events we used a robust threshold. We validated our threshold approach by attributing extreme events found in the conductivity to historical volcanic eruptions in Sigl et al. (2013). This also confirms our dating approach since the year of the eruption matched the year of occurrence in the ice core record.

For conductivity and ammonium the signal to noise ratio is high enough to detect a sufficient number of extreme events. However, not all events at the source region that could lead to extremely high concentration in the ice core record are detected in the ice core record. This is caused by the need of prevailing atmospheric circulation bringing the aerosols to Greenland. Also scavenging en-route during the transport changes the composition. Nevertheless, we are able to provide a reliable picture of relative changes in extremes over a sufficient time period. As the conductivity is a bulk parameter, it is difficult to draw further conclusion from its number of extreme events. However, we attributed more than half of the extreme events found in conductivity to volcanic eruptions and we assume from previous studies that some wildfires are also depicted in the conductivity record (Leuenberger, 2013). Leuenberger (2013) used the threshold approach to examine the fire frequency in the ammonium record of the NEEM ice core. Relatively high peaks in ammonium can be

attributed to wildfire events, however, only very few wildfire events are detected in the Greenland ice (Fuhrer et al., 1996; Legrand et al., 2016; Leuenberger, 2013). Legrand et al. (2016) reported a high fire frequency from 1050 to 1450. Leuenberger (2013) also states that higher ammonium concentration can be caused by volcanic eruptions recorded in the ice core. We did not account for this effect and set a slightly different threshold, which could lead to a higher number of extreme event occurrence found in our analysis. When comparing our results to Leuenberger (2013), it is difficult to draw conclusions about the changes in ammonium concentrations since the time period of our ammonium record is too short due to data quality issues.

It is difficult to draw conclusions from the extreme events in calcium and sodium since the number of extreme events is small. However, we assume that calcium and sodium concentration depict natural background concentration and might not be influenced by anthropogenic emissions. Additionally, the frequency of occurrence of extreme events in calcium and sodium is relatively stable over time. For calcium and sodium, storms have a major influence on bringing the aerosols up into the atmosphere (Rhodes et al., 2018; Sun et al., 2001). Further, the calcium or sodium aerosols need to be transported to the study site. Therefore, we need prevailing wind and storm pathways that bring the aerosols to northeast Greenland. For sodium, as already mentioned before, scavenging-en route might lead to extraordinary low concentrations detected at the study site. This could be the reason why we detect more low concentration extreme events than high concentration extreme events. However, since the difference between the detection of extremely low and high extreme events is small, we conclude that effects leading to an extremely high loss of sodium caused by scavenging-en route are rare but may be more pronounced before 1200 AD. The frequency of occurrence of extreme events in calcium and sodium is relatively stable over time with a slight increase in the 15th and 16th century. Schüpbach et al. (2018) compared the Eemian to the Holocene calcium concentration correcting for loss processes during transport. They found slightly higher dust aerosol concentrations at the source during the Eemian pointing at higher dust mobilization, hence aridity and/or wind speed in the Asian desert regions at that time. Therefore, the increase in calcium extreme events from 1400 to 1600 AD might also be attributed to drier conditions and dust storm activity in East Asian deserts.

A higher frequency of extreme event occurrence in conductivity coincides with higher extreme event frequency in ammonium. Since the conductivity is a bulk parameter we might be able to attribute the increase in conductivity to an increase in wildfire events depicted in the ammonium record. A high number of occurrence of extreme events in nitrate might be attributed to an increase of biomass burning or lightning events. Therefore, high numbers of extreme events in ammonium and nitrate could coincide with warmer and drier climatic conditions during this time. However, Nitrate is also affected by post-depositional loss since it is reversibly incorporated in the snow pack (Fischer et al., 1998). The layer thickness is slightly higher during the period of an increased number of extreme event occurrence. A higher accumulation leads to a decreased loss of nitrate in the snow. Therefore, not only an increase of

lightning and biomass burning at the source region but also changes at the deposition site can potentially influence the change in frequency.

4.2 Comparison with other Ice Cores

Sea salt is a perfect indicator for atmospheric circulation since it is not influenced by anthropogenic impacts. In the following part, we discuss the EGRIP S6, Tunu and NEGIS ice core sodium concentrations. All records show high annual variability over the time period that are hardly consistent on a year to year basis in all three records as they do not show synchronous interannual variability. This inconsistency can be attributed to two main reasons. First, variability in the scavenging of the atmospheric aerosols. A high sea salt concentration often suggests high storm activity and is therefore related to cyclonic activity (Fischer, 2001). This however implies that differences in storm track pathway and local precipitation activity can alter the aerosol deposition. Second, post-depositional changes of the snow pack mostly through wind drift reworking the snow strata. This leads to a change in signal-to-noise ratio especially in low accumulation areas like in the Northeast Greenland region (Fischer, 2001). The signal-to-noise ratio was increased by averaging the sodium data with an 11-year window. Additionally, we tried to eliminate possible changes in the accumulation rate, which is influenced by post-depositional processes as well as errors in the age scale by using smoothed data as it was also done in other studies (Appenzeller et al., 1998; Crüger et al., 2004). This process reduces the high frequency variability.

Gfeller et al. (2014) found that spatial representation decreases with distance between the drilling sites. The representativeness decorrelates from 60 cm to 10 m. Therefore, a rather low correlation is expected from ice cores being further apart than 10 m on an interannual basis. However, the correlation between two ice core records stays relatively stable in a distance of 10 m to 3 km. This also supports the importance of processes during and after the deposition of aerosols. Gfeller et al. (2014) did not make an analysis about ice core sites being further apart than 3 km where unevenly distributed deposition due to local, individual precipitation events is important. Further, they investigated around the NEEM study site with an accumulation rate of around 26 cm per year and only looked at inter-annual timescales. Further, Gfeller et al. (2014) argues by several ice cores within the above mentioned distance the representativeness can be increased.

We would expect that variability in the post-depositional changes is less influenced, whereas variability caused by scavenging is more influenced by the distance between the study locations. Interestingly, we found a statistically significant correlation between Tunu and NEGIS as well as Tunu and EGRIP S6 sodium records which are about 300 km apart. However, the ice cores are only statistically significant on the 10% level but not statistically significant on the 5% level. No statistically significant correlation between EGRIP S6 and NEGIS, which are only about 1 km apart, could be found. Dry and wet deposition regimes are both important for an accumulation rate of around 10 cm per year as experienced in northeast Greenland

(Hutterli et al., 2007). Since single cyclonic events mostly influence the accumulation rate in Northeast Greenland, regional individual precipitation events have a high impact on the aerosol concentration. It is remarkable that the Tunu sodium record has a higher correlation coefficient with the EGRIP S6 and NEGIS sodium record given that its study site is further away from the NEGIS and EGRIP S6 study site than these are to each other. Especially when considering that NEGIS and EGRIP S6 should be influenced by the same local weather leading to the same aerosol concentration deposition. This supports the hypothesis that processes after deposition can play a major role as surface topography and wind blowing lead to inter site variability in snow concentration (Fischer, 2001). This however cannot fully explain the difference in correlation. We did not have annual layers for the NEGIS ice core. Therefore, when looking on an inter-annual scale it is possible that the concentrations of an annual layer of the NEGIS sodium record are not correct. We tried to reduce this by averaging over an 11-year window. However, since we further did not account for differences in layer thickness, this could be one of the major reasons for the non-significant correlation.

4.3 Comparison with Atmospheric and Oceanic Circulation Patterns

We use the variability in ice core impurity time series in order to link potential variations in climate indices, which are representing atmospheric circulation patterns, to the ice core record. As already mentioned in *4.2* changes in en-route scavenging and transport speed can lead to concentration changes in the ice that are not representative of source variability. Additionally, post-depositional processes play a major role in the variability of the aerosol concentration in the ice core record. Since we focus on changes in en-route transport by correlating the ice core record with climate indices, it is particularly difficult to relate these changes in transport to changes in the aerosol concentration in the ice. The atmospheric signal in the ice needs to dominate over the depositional noise in the ice core record in order to reconstruct the atmospheric interannual variability. This cannot be done reliably by only using one single ice core which was already stated by Gfeller et al. (2014). Nevertheless, by keeping this in mind, we try to interpret the statistically significant correlations and try to explain why non-significant correlations appear.

The NAO is a measure of storminess and therefore of the cyclonic activity for the North Atlantic region. We argued that the NAO might have an influence on the sodium source region which is a tracer for sea salt which is already mentioned in *4.2*. It is supposed to be influenced by high storm activity and is therefore related to cyclonic activity (Fischer, 2001). The correlation of the NAO and the sodium record comprises both: Efficient generation and uplift of sea salt within frontal systems and the guidance of storm tracks by large-scale pressure patterns in the North Atlantic region onto the ice sheets. According to Serreze et al. (1997) lower pressure fields above Iceland lead to higher storm activity above the Northeast Atlantic, and therefore bring more sea salt into the upper atmosphere. These situations are typical for the positive phase of the NAO. We cannot find a significant connection between a pressure pattern resembling

the NAO and sodium concentration in our correlation analysis. Generally, the NAO index and our ice core record are influenced by interannual variations with a low signal-to-noise ratio and a non-linear relationship. Therefore, we cannot find a correlation between the station-based NAO and sodium in the ice core.

Additionally, we argue that the positive NAO phase is related to a northward shift of the jet stream, which can transport aerosols in the atmosphere and is related to a higher cyclonic activity in northeastern Greenland (Hurrell, 1995). Higher cyclonic activity in the northeastern Greenland region could lead to an increase of precipitation events in Northeast Greenland and would influence the concentrations of all aerosols by scavenging. However, this process could be diminished by dilution effects during heavy precipitation events.

There are other possible explanations why we find no correlation between the sea salt export or the general aerosol transportation and the NAO index. In general, dating errors hamper the correlation on an inter annual time scale. Additionally, the station based NAO index does not depict dynamic effects. Therefore, it might not be a good representation for the atmospheric circulation. This is supported by Hutterli et al. (2005) relating northeast Greenland accumulation variability to the local cyclone frequency rather than to a quasi-stationary distinct large-scale circulation pattern.

Fischer & Mieding (2005) found a correlation of sea salt and SST and related this to an indirect effect of SST and storm activity as well as pressure distribution over the North Atlantic. This atmosphere ocean coupling is found in model studies (Delworth & Mann, 2000). Fischer & Mieding (2005) related elevated sea salt concentrations to a northward shift of storm tracks over the Atlantic that are influenced by long-term variability in SST. The AMO is a measure of long-term changes in SST in the North Atlantic region. We tried to find a correlation between the AMO and our aerosol record. By using the running mean, we averaged over a long time period leading to a reduced noise level. Generally, decadal variations in the aerosols are less affected by dating errors or depositional noise leading to significant correlation with the AMO index. Therefore, we diminished the dating error since it is substantially smaller than the time scale of these changes. For the AMO index we have to differentiate between the short AMO index that is based on instrumental measurements and the long AMO index that is based on proxy reconstruction before the time period when instrumental data became available. For calcium and sodium, both indices show a negative sign in correlation. Additionally, the AMO might be linked to the NAO which in turn might lead to higher storminess for the positive NAO pattern during negative AMO phases. Higher storminess would support the outcome of Fischer & Mieding (2005) stating that a low pressure over the Greenland sea is connected to enhanced cyclonic activity entering the Greenland ice. This comes in line with our outcome since a negative AMO leads to higher storminess and more cyclones transporting aerosols to the Northeast Greenland region, therefore we get a higher concentration of the aerosols. The higher concentration could also be influenced by precipitation events efficiently washing out the aerosols in the air leading to higher

concentration in the accumulated snow. For nitrate, the short and long AMO index show the opposite sign in correlation where only the correlation with the short AMO index is significant on the 5% level. As the time interval covered by the short AMO coincides with the anthropogenic NO_3^- increase this correlation may be fortuitous.

The PDO and the calcium record are not significantly correlated even after averaging over a running window of 11 years to reduce the noise level. Our outcome is in line with Fischer & Mieding (2005) who did not find a clear signal in SST anomalies in the Pacific region. This might be explained by low influences of the PDO on the atmospheric circulation around Greenland and therefore on the ice core record.

Generally, we can conclude that the NAO, short AMO and PDO indices are not well represented in the EGRIP S6 ice core record by only looking at one single ice core. However, this representation can be improved to a certain degree by averaging as can be seen for sodium, calcium and nitrate. Additionally, we invoke a linear relationship between the aerosol concentration and the climate indices, which might not be the case. Further, we give an outlook on potential measures to increase the atmospheric signal depicted in Greenland ice core record.

5 Outlook

This section will give a further outlook on measures that can be taken to improve our analysis. We propose the following possible course of action to be able to make further progress in studying decadal to interannual variations depicted in ice core records for the northeastern Greenland region and especially the EGRIP site. It is necessary to increase the number of ice core samples to be able to make accurate prediction of the transport path to the northeastern Greenland region. To make representative predictions, it is necessary to quantify the depositional noise by drilling these ice cores within a certain distance. Gfeller et al. (2014) suggested this distance to be within a range of minimum 1 m not to calculate erroneously high representativeness and not further than 10 m from the drill site since this would decrease the correlation. With cross correlating between the ice cores this will diminish the variability from interannual noise that is not caused by atmospheric circulation patterns. It is also possible to use other methods to detect atmospheric circulation patterns above northeast Greenland e.g. methods based on reanalysis data (Fischer 2005) that do not invoke a linear relationship. This would also obliviate the effect of only looking at stationary atmospheric patterns which only depict a portion of the atmospheric circulation.

Additionally, a more accurate annual layer count needs to be implemented to eliminate the interval where the annual layer thickness of the EGRIP S6 ice core was elevated. Therefore, the Straticounter algorithm needs to be revised to better represent the annual layer thickness during data gaps (Winstrup et al., 2012). Furthermore, the GICCO5 timescale could be applied to the NEGIS and Tunu ice core to improve the correlation analysis. However, as soon as more ice cores around the EGRIP study site are available, it is more applicable to correlate the NEGIS and EGRIP S6 ice core to these ice cores than to the Tunu ice core. This would diminish the effect of unevenly distributed precipitation leading to different concentration.

For the stability in nitrate stringent care of the system is required when handling the nitrate in order to ovoid drift in the data. Further, there needs to be further investigation on the analytical problems which might be caused by contamination in ammonium before the bubble close-off.

References

Alley, R. B., Finkel, R. C., Nishiizumi, K., Anandakrishnan, S., Shuman, C. A., Mershon, G., … Mayewski, P. A. (1995). Changes in continental and sea-salt atmospheric loadings in central Greenland during the most recent deglaciation: Model-based estimates. Journal of Glaciology, 41(139), 503–514.

Appenzeller, C., Schwander, J., Sommer, S., & Stocker, T. F. (1998). The North Atlantic Oscillation and its imprint on precipitation and ice accumulation in Greenland. Geophysical Research Letters, 25(11), 1939–1942.

Bigler, M., Svensson, A., Kettner, E., Vallelonga, P., Nielsen, M. E., & Steffensen, J. P. (2011). Optimization of high-resolution continuous flow analysis for transient climate signals in ice cores. Environmental Science & Technology, 45(10), 4483–4489.

Biscaye, P. E., Grousset, F. E., Revel, M., Van der Gaast, S., Zielinski, G. A., Vaars, A., & Kukla, G. (1997). Asian provenance of glacial dust (stage 2) in the Greenland Ice Sheet Project 2 ice core, Summit, Greenland. Journal of Geophysical Research: Oceans, 102(C12), 26765–26781.

Bory, A.-M., Biscaye, P. E., Svensson, A., & Grousset, F. E. (2002). Seasonal variability in the origin of recent atmospheric mineral dust at NorthGRIP, Greenland. Earth and Planetary Science Letters, 196(3–4), 123–134.

Bory, A. J., Biscaye, P. E., & Grousset, F. E. (2003). Two distinct seasonal Asian source regions for mineral dust deposited in Greenland (NorthGRIP). Geophysical Research Letters, 30(4).

Crüger, T., Fischer, H., & von Storch, H. (2004). What do accumulation records of single ice cores in Greenland represent? Journal of Geophysical Research: Atmospheres, 109(D21).

Delworth, T. L., & Mann, M. E. (2000). Observed and simulated multidecadal variability in the Northern Hemisphere. Climate Dynamics, 16(9), 661–676.

Du, Z., Xiao, C., Zhang, Q., Li, C., Wang, F., Liu, K., & Ma, X. (2019). Climatic and environmental signals recorded in the EGRIP snowpit, Greenland. Environmental Earth Sciences, 78(5), 170.

Erhardt, T. (2013). A 3000 Year High Resolution Dust Record from the NEEM Ice Core. Retrieved from www.climatestudies.unibe.ch/students/theses/msc/109.pdf

Erhardt, T., Jensen, C. M., Borovinskaya, O., & Fischer, H. (2019). Single Particle Characterization and Total Elemental Concentration Measurements in Polar Ice Using Continuous Flow Analysis-Inductively Coupled Plasma Time-of-Flight Mass Spectrometry. Environmental Science & Technology, 53(22), 13275–13283.

Fischer, H. (2001). Imprint of large-scale atmospheric transport patterns on sea-salt records in northern Greenland ice cores. Journal of Geophysical Research Atmospheres, 106(D20), 23977–23984.

Fischer, H., Fundel, F., Ruth, U., Twarloh, B., Wegner, A., Udisti, R., … Severi, M. (2007). Reconstruction of millennial changes in dust emission, transport and regional sea ice coverage using the deep EPICA ice cores from the Atlantic and Indian Ocean sector of Antarctica. Earth and Planetary Science Letters, 260(1–2), 340–354.

Fischer, H., & Mieding, B. (2005). A 1,000-year ice core record of interannual to multidecadal variations in atmospheric circulation over the North Atlantic. Climate Dynamics, 25(1), 65–74.

Fischer, H., Schüpbach, S., Gfeller, G., Bigler, M., Röthlisberger, R., Erhardt, T., … Wolff, E. W. (2015). Millennial changes in North American wildfire and soil activity over the last glacial cycle. Nature Geoscience, 8(9), 723–727.

Fischer, H., Wagenbach, D., & Kipfstuhl, J. (1998a). Sulfate and nitrate firn concentrations on the Greenland ice sheet: 1. Large-scale geographical deposition changes. Journal of Geophysical Research: Atmospheres, 103(D17), 21927–21934.

Fischer, H., Wagenbach, D., & Kipfstuhl, J. (1998b). Sulfate and nitrate firn concentrations on the Greenland ice sheet: 2. Temporal anthropogenic deposition changes. Journal of Geophysical Research: Atmospheres, 103(D17), 21935–21942.

Fuhrer, K., Neftel, A., Anklin, M., & Maggi, V. (1993). Continuous measurements of hydrogen peroxide, formaldehyde, calcium and ammonium concentrations along the new GRIP ice core from Summit, Central Greenland. Atmospheric Environment. Part A. General Topics, 27(12), 1873–1880.

Fuhrer, K., Neftel, A., Anklin, M., Staffelbach, T., & Legrand, M. (1996). High-resolution ammonium ice core record covering a complete glacial-interglacial cycle. Journal of Geophysical Research Atmospheres, 101(D2), 4147–4164.

Gfeller, G., Fischer, H., Bigler, M., Schüpbach, S., Leuenberger, D., & Mini, O. (2014). Representativeness and seasonality of major ion records derived from NEEM firn cores. The Cryosphere, 8(5), 1855–1870.

Gow, A. J. (1965). On the accumulation and seasonal stratification of snow at the South Pole. Journal of Glaciology, 5(40), 467–477.

Grigholm, B., Mayewski, P. A., Kang, S., Zhang, Y., Kaspari, S., Sneed, S. B., & Zhang, Q. (2009). Atmospheric soluble dust records from a Tibetan ice core: Possible climate proxies and teleconnection with the Pacific Decadal Oscillation. Journal of Geophysical Research, 114(D20), 1–13.

Herron, M. M., & Langway, C. C. (1980). Firn densification: an empirical model. Journal of Glaciology, 25(93), 373–385.

Hobbs, W. W. (1945). The greenland gllacial anticyclone. Journal of Meteorology, 2(3), 143–153.

Hurell, J. (2001). The North Atlantic Oscillation: Climatic Significance and Environmental Impacts. National Center for Atmospheric Research.

Hurrell, J. W. (1995). Decadal Trends in the North Atlantic Oscillation: Regional Temperatures and Precipitation. Science, 269(5224), 676–679.

Hutterli, M. A., Crueger, T., Fischer, H., Andersen, K. K., Raible, C. C., Stocker, T. F., … Burkhart, J. F. (2007). The influence of regional circulation patterns on wet and dry mineral dust and sea salt deposition over Greenland. Climate Dynamics, 28(6), 635–647.

Hutterli, M. A., Raible, C. C., & Stocker, T. F. (2005). Reconstructing climate variability from Greenland ice sheet accumulation: An ERA40 study. Geophysical Research Letters, 32(23), 1–4.

Kahl, J. D. W., Martinez, D. A., Kuhns, H., Davidson, C. I., Jaffrezo, J., & Harris, J. M. (1997). Air mass trajectories to Summit, Greenland: A 44-year climatology and some episodic events. Journal of Geophysical Research: Oceans, 102(C12), 26861–26875.

Kaufmann, P. R., Federer, U., Hutterli, M. A., Bigler, M., Schüpbach, S., Ruth, U., … Stocker, T. F. (2008). An improved continuous flow analysis system for high-resolution field measurements on ice cores. Environmental Science & Technology, 42(21), 8044–8050.

Legrand, M., & Mayewski, P. (1997). Glaciochemistry of polar ice cores: a review. Reviews of Geophysics, 35(3), 219–243.

Legrand, M., McConnell, J., Fischer, H., Wolff, E. W., Preunkert, S., Arienzo, M., … Place, P. (2016). Boreal fire records in Northern Hemisphere ice cores: a review. Climate of the Past, 12(10), 2033–2059.

Leuenberger, D. (2013). The High Resolution NEEM Aerosol Records Over the Last 3000 Years : A New Approach to Determine Wildfire Frequency.

Mann, M. E., Zhang, Z., Rutherford, S., Bradley, R. S., Hughes, M. K., Shindell, D., … Ni, F. (2009). Global signatures and dynamical origins of the Little Ice Age and Medieval Climate Anomaly. Science, 326(5957), 1256–1260.

Mantua, N. J., & Hare, S. (2002). Pacific-Decadal Oscillation (PDO). Encyclopedia of Global Environmental Change, 1, 592–594.

Maselli, O. J., Chellman, N. J., Grieman, M., Layman, L., McConnell, J. R., Pasteris, D., … Sigl, M. (2017). Sea ice and pollution-modulated changes in Greenland ice core methanesulfonate and bromine. Climate of the Past, 13(1), 39–59.

McConnell, J. R., Lamorey, G. W., Lambert, S. W., & Taylor, K. C. (2002). Continuous ice-core chemical analyses using inductively coupled plasma mass spectrometry. Environmental Science & Technology, 36(1), 7–11.

Merz, N., Raible, C., Fischer, H., Varma, V., Prange, M., & Stocker, T. (2013). Greenland accumulation and its connection to the large-scale atmospheric circulation in ERA-Interim and paleoclimate simulations. Climate of the Past, 9(6), 2433–2450.

Mojtabavi, S., Wilhelms, F., Cook, E., Davies, S., Sinnl, G., Jensen, M. S., … Rasmussen, S. O. (2019). A first chronology for the East GReenland Ice – core Project (EGRIP) over the Holocene and last glacial termination. Climate of the Past Discussions, in review.

Mudelsee, M. (2014). Extreme value time series. In Climate Time Series Analysis (pp. 217–267). Springer.

Pandis, S. N., & Seinfeld, J. H. (2006). Atmospheric chemistry and physics: From air pollution to climate change. Wiley.

Rasmussen, S. O., Abbott, P. M., Blunier, T., Bourne, A. J., Brook, E. J., Buchardt, S. L., … Cook, E. (2013). A first chronology for the North Greenland Eemian Ice Drilling (NEEM) ice core. Climate of the Past, 9(6).

Rhodes, R. H., Yang, X., & Wolff, E. W. (2018). Sea ice versus storms: what controls sea salt in Arctic ice cores? Geophysical Research Letters, 45(11), 5572–5580.

Roe, G. H. (2005). Orographic precipitation. Annu. Rev. Earth Planet. Sci., 33, 645–671.

Röthlisberger, R., Bigler, M., Hutterli, M., Sommer, S., Stauffer, B., Junghans, H. G., & Wagenbach, D. (2000). Technique for continuous high-resolution analysis of trace substances in firn and ice cores. Environmental Science & Technology, 34(2), 338–342.

Schüpbach, S., Fischer, H., Bigler, M., Erhardt, T., Gfeller, G., Leuenberger, D., … Fleet, L. (2018). Greenland records of aerosol source and atmospheric lifetime changes from the Eemian to the Holocene. Nature Communications, 9(1), 1–10.

Serreze, M. C., Carse, F., Barry, R. G., & Rogers, J. C. (1997). Icelandic low cyclone activity: Climatological features, linkages with the NAO, and relationships with recent changes in the Northern Hemisphere circulation. Journal of Climate, 10(3), 453–464.

Sigg, A., Fuhrer, K., Anklin, M., Staffelbach, T., & Zurmuehle, D. (1994). A continuous analysis technique for trace species in ice cores. Environmental Science & Technology, 28(2), 204–209.

Sigl, M., McConnell, J. R., Layman, L., Maselli, O., McGwire, K., Pasteris, D., … Edwards, R. (2013). A new bipolar ice core record of volcanism from WAIS Divide and NEEM and implications for climate forcing of the last 2000 years. Journal of Geophysical Research: Atmospheres, 118(3), 1151–1169.

Sun, J., Zhang, M., & Liu, T. (2001). Spatial and temporal characteristics of dust storms in China and its surrounding regions, 1960–1999: Relations to source area and climate. Journal of Geophysical Research: Atmospheres, 106(D10), 10325–10333.

Svensson, A., Andersen, K. K., Bigler, M., Clausen, H. B., Dahl-Jensen, D., Davies, S. M., … Röthlisberger, R. (2006). The Greenland ice core chronology 2005, 15–42 ka. Part 2: comparison to other records. Quaternary Science Reviews, 25(23–24), 3258–3267.

Team, R. C. (2018). R Foundation for Statistical Computing; Vienna, Austria: 2015. R: A Language and Environment for Statistical Computing, 2013.

Vallelonga, P., Christianson, K., Alley, R. B., Anandakrishnan, S., Christian, J. E. M., Dahl-Jensen, D., … Karlsson, N. B. (2014). Initial results from geophysical surveys and shallow coring of the Northeast Greenland Ice Stream (NEGIS). The Cryosphere, 8(4), 1275–1287.

Vinther, B. M., Clausen, H. B., Johnsen, S. J., Rasmussen, S. O., Andersen, K. K., Buchardt, S. L., … Steffensen, J. P. (2006). A synchronized dating of three Greenland ice cores throughout the Holocene. Journal of Geophysical Research: Atmospheres, 111(D13).

Wagenbach, D., Ducroz, F., Mulvaney, R., Keck, L., Minikin, A., Legrand, M., … Wolff, E. W. (1998). Sea-salt aerosol in coastal Antarctic regions. Journal of Geophysical Research: Atmospheres, 103(D9), 10961–10974.

Winstrup, M., Svensson, A. M., Rasmussen, S. O., Winther, O., Steig, E. J., & Axelrod, A. E. (2012). An automated approach for annual layer counting in ice cores. Climate of the Past Discussions, 8(6), 1881–1895.

Yang, X., Pyle, J. A., & Cox, R. A. (2008). Sea salt aerosol production and bromine release: Role of snow on sea ice. Geophysical Research Letters, 35(16).

Appendix

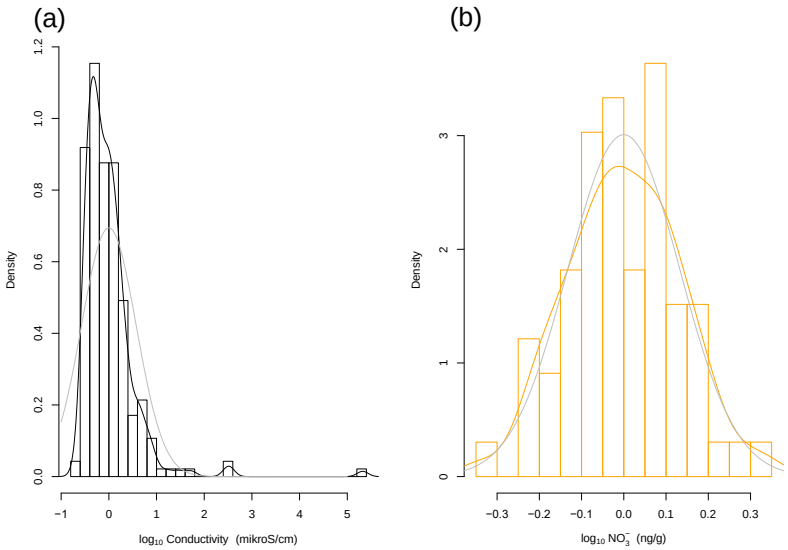

Figure 20 Density plots of the logarithm of the residuals of the linear regression of (a) conductivity and (b) nitrate concentrations with their standard normal distribution (grey line) and their histograms (bar plot). Conductivity has a higher peak and nitrate is skewed towards higher values compared to a normal distribution.

Table 3 depicts the list of historic volcano eruptions (column 1) with the start and end of the eruption (column 2-3), the detected year by the threshold method (column 4) and the detection error in (column 5). * indicates volcanoes which are the most likely or possible candidates for the cause of extreme conductivity concentrations.

Historic Volcano Eruptions	Start of Eruption	End of Eruption	Detected in Year	Detection Error
Katmai, Alaska	1912.8	1914.7	1912.2	
Krakatoa, ID	1883.6	1886.3	1885.0	
Grímsvötn, IS*	1872.6	1873.5	1873.4	
Tambora, ID	1815.6	1817.6	1817.4	
Unknown	1809.7	1811.2	1810.5	
Grímsvötn, IS	1782.8	1784.5	1784.0	
Tarumai, JP*	1739.0	1740.6	1741.8	
Lanzarote, SP*	1729.2	1732.5	1732.9	
Unknown	1695.0	1696.3	1695.2	
Tarumai, JP*	1667.6	1668.5	1667.9	
Parker Peak, PH	1641.1	1643.3	1642.3	
Huaynaputina, PU	1601.1	1603.1	1601.2	
Ruiz, CO*	1595.1	1597.4	1595.7	
Unknown	1567.4	1568.4	1568.8	+1
Augustine, Alaska*	1537.2	1538.3	1537.8	
Hekla, IS*	1512.4	1513.0	1512.8	
Katla, IS*	1502.5	1503.1	1503.8	+1

Bardarbunga, IS*	1476.8	1478.2	1477.1	
Sakura Jima, JP*	1470.8	1470.8	1470.8	
Unknown	1459.1	1461.4	1459.7	
Unknown	1453.1	1454.2	1453.5	
Unknown	1344.9	1347.3	1347.1	
Unknown	1286.8	1289.6	1288.2	
Samalas, ID	1258.2	1260.6	1259.5	
Unknown	1229.3	1232.5	1231.2	
Unknown	1168.1	1170.2	1169.2	
Unknown	1104.9	1108.6	1107.1	

Acknowledgements

I would like to thank…

...Prof. Hubertus Fischer, my supervisor, for giving me the chance to work in his team, his support and the supervision of this thesis.

…Dr. Tobias Erhardt, co-supervisor for my Master Thesis, for the introduction to the CFA and for your patient explanations.

...Fortunat Joos for chairing the defense.

…my friend, office maid and proofreading fairy Chantal Zeppenfeld.

…Friedrich Burger, Dr. Jonathan Buzan, Alexandre Mösching and Camilla Jansen for your patient explanations and input that helped me reflect my work.

...the Bern Ice Core Group for the good atmosphere during lunchbreaks.

...Doris Rätz for the administrative work and Gunnar Jansen for the IT support.

…Jennifer Pappert for her excellent proofreading skills.

…people of KUP for interesting discussions, entertaining coffee breaks and the other good moments after work.

…my family and friends for always being there for me.

Declaration of consent

on the basis of Article 30 of the RSL Phil.-nat. 18

Name/First Name: Link/Kathrine Mia

Registration Number: 18-120-428

Study program: Climate Sciences qualification in Climate and Earth System Science

Bachelor ☐ Master ☑ Dissertation ☐

Title of the thesis: Study of Extreme Events in Millennial Aerosol Records from Greenland

Supervisor: Prof. Dr. H. Fischer
Dr. T. Erhardt

I declare herewith that this thesis is my own work and that I have not used any sources other than those stated. I have indicated the adoption of quotations as well as thoughts taken from other authors as such in the thesis. I am aware that the Senate pursuant to Article 36 paragraph 1 litera r of the University Act of 5 September, 1996 is authorized to revoke the title awarded on the basis of this thesis.
For the purposes of evaluation and verification of compliance with the declaration of originality and the regulations governing plagiarism, I hereby grant the University of Bern the right to process my personal data and to perform the acts of use this requires, in particular, to reproduce the written thesis and to store it permanently in a database, and to use said database, or to make said database available, to enable comparison with future theses submitted by others.

Bern/ 28/02/2020

Place/Date

Signature